# ASSESSMENT OF EFFECTS OF BOTULINUM TOXIN ON MUSCLE MECHANICS

by

**Ahu Nur Türkoğlu**

B.Sc., Physics, Boğaziçi University, 2008

M.Sc., Biomedical Engineering, Boğaziçi University, 2010

Submitted to the Institute of Biomedical Engineering

in partial fulfillment of the requirements

for the degree of

Doctor

of

Philosophy

Boğaziçi University

2016

# ASSESSMENT OF EFFECTS OF BOTULINUM TOXIN ON MUSCLE MECHANICS

## APPROVED BY:

Prof. Dr. Can Ali Yücesoy .....
(Thesis Advisor)

Prof. Dr. Cengizhan Öztürk .....

Assoc. Prof. Dr. Burak Güçlü .....

Assoc. Prof. Dr. Ekin Akalan .....

Assist. Prof. Dr. Bora Garipcan .....

**DATE OF APPROVAL:** 14 September 2015

# ACKNOWLEDGMENTS

Firstly, I would like to express my sincere gratitude to my advisor Prof. Dr. Can A. Yücesoy for the continuous support of my Ph.D. study and related research, for his patience, motivation, and immense knowledge. His guidance helped me in all the time of research and writing of this thesis.

Besides my advisor, I would like to thank the rest of my thesis committee: Prof. Dr. Cengizhan Öztürk, Assoc. Prof. Dr. Burak Güçlü, Assist. Prof. Dr. Bora Garipcan and Assoc. Prof. Dr. Ekin Akalan, for their insightful comments and encouragement, but also for the question which incented me to widen my research from various perspectives.

I thank my fellow labmates, Filiz Ateş, Uluç Pamuk, Alper Yaman, Önder Emre Arıkan, Selen Ersoy, Gizem Sarıbaş, Agah Karakuzu, Orkun Akcan, in for all the support they gave and for all the fun we have had.

Many friends have helped me stay sane through these difficult years. I owe special thanks my friends Filiz Ateş, Berre Gümüş, Nermin Topaloğlu, Didar Talat, Burcu Tunç, Fatma Temiz, Esin Karahan, Murat Tümer, Bora Büyüksaraç, Bige Vardar, Ismail Devecioğlu, Muhammed Avşar, Özgür Kaya, Gamze Ateş, Neslihan Sarıca, Eda Çapa, Özgür Tabakoğlu with whom we crossed paths at the Institute of Biomedical Engineering. Their support and care helped me overcome setbacks and stay focused on my graduate study. I greatly value their friendship and I deeply appreciate their belief in me.

I also would like to thank my precious "dostlarım" Filiz Ateş, Oktay Büyükkeskin and Ece Ercan. I warmly appreciate the generosity and understanding of my extended family.

Most importantly, none of this would have been possible without the love and patience of my mother. My mother, Peruzat Türkoğlu to whom this dissertation is dedicated to, has been a constant source of love, concern, support and strength all these years. I would like to express my heart-felt gratitude to her.

# ACADEMIC ETHICS AND INTEGRITY STATEMENT

I, Ahu Nur Türkoğlu, hereby certify that I am aware of the Academic Ethics and Integrity Policy issued by the Council of Higher Education (YÖK) and I fully acknowledge all the consequences due to its violation by plagiarism or any other way.

Name :

Signature:

Date:

# ABSTRACT

## ASSESSMENT OF EFFECTS OF BOTULINUM TOXIN ON MUSCLE MECHANICS

Effects of widely used Botulinum toxin (BTX) treatment on muscular mechanics are highly important, but their mechanism and time course are not well understood. Present thesis is focused on mechanical mechanism of BTX treatment using finite element method and animal experiments. In an isolated muscle model partial paralyzation is shown to cause (i) the sarcomeres to attain higher lengths throughout the entire muscle (e.g., at short muscle length, the inactivated fascicles of middle half paralyzed muscle and the same parts within BTX-free muscle shortened by 29-27% and 32-29%, respectively), (ii) enhanced potential of active force production of the non-paralyzed muscle parts (up to 14.5% for BTX cases), and (iii) decreased muscle length range of force exertion. It is shown that intramuscular myofascial force transmission is central to these effects. Additionally, experimental results showed diminished epimuscular MFT and intramuscular collagen increase. Due to information on the loss of interactions between muscles and increased ECM stiffness due to increased collagen, temporal changes within the muscle during treatment is examined. Modeling of time course of the BTX treatment showed that sarcomeres attain even higher lengths with increased ECM stiffness and is reversed at longer muscle lengths. Consequently, force production capacity of activated sarcomeres gets further enhanced in the long-term and a narrower length range of force exertion (20.3%, 27.1% and 3.4%, acute, long-term and post BTX treatment, respectively) is a consistent finding. If such stiffness increase were shown to remain post-treatment, enhanced capacity would become permanent for the entire muscle. It is concluded that mechanical effects and morphological changes shown can affect muscular mechanics adversely if not managed accordingly.

**Keywords:** Botulinum toxin, Myofascial force transmission, Finite element modeling, length-force characteristics, longer sarcomere effect, time course of BTX.

# ÖZET

## BOTULİNUM TOKSİN'İN KAS MEKANİĞİNE ETKİLERİNİN DEĞERLENDİRİLMESİ

Yaygın olarak kullanılan Botulinum Toksin tedavisinin kas mekaniği üzerindeki etkileri oldukça önemlidir fakat bu etkilerin mekanizması ve süreci bilinmemektedir. Bu tez, sonlu elemanlar analizi ve hayvan deneyleri kullanarak BTX tedavisinin mekanik etkileri üzerine odaklanmıştır. Izole kas modelinde kısmi paralizasyonun (i) tüm kas boyunca daha uzun boy değerleri almasına (ör. kısa boyda orta kısmı paralize edilmiş kasın inaktif kısmı ile BTX olmayan kas modelinin aynı kısımları sırasıyla 29-27% ve 32-29% oranında kısalmışlardır.), (ii) aktif kuvvet üretimi potansiyelinde artışa (BTX durumlarında 14.5%'a kadar), (iii) kas etkime boyunda kısalamaya neden olduğu gösterilmiştir. Bu etkilerin temelinde miyobağdokusal kuvvet iletimi olduğu gösterilmiştir. Ek olarak, deneysel sonuçlarda epimüsküler MFT'de azalma ve intramüsküler kolajen miktarında artış gözlenmiştir. Kaslar arasındaki bu etkileşim kaybı ve kolajen miktarındaki artış sonucu ECM sertleşmesi nedeni ile tedavi sırasında kasta oluşacak değişimler ele alınmıştır. BTX tedavisinin zaman içerisindeki etkilerinin modellenmesi sarkomerlerin ECM sertliğindeki artış ile daha uzun boy değerleri aldığını ve uzun boyda bu etkinin tersine döndüğünü göstermiştir. Dolayısıyla aktif sarkomerlerin kuvvet üretim potansiyeli artışı ve kas etkime aralığındaki daralma bulguları istikrarlı olarak bulunmuştur (akut, uzun dönem ve BTX sonrası durumlarında sırasıyla 20.3%, 27.1% ve 3.4%). Sertlik artışının tedavi sonrasında kalıcı olması durumunda kuvvet üretme potansiyelindeki artış da kalıcı olacaktır. Mekanik ve morfolojik etkilerin doğru yönetilmemesinin tedaviyi olumsuz yönde etkileyeceği sonucuna ulaşılmıştır.

**Anahtar Sözcükler:** Miyobağdokusal kuvvet iletimi, Botulinum toksin, Sonlu elemanlar modellemesi, boy-kuvvet ilişkisi, Uzun sarkomer etkisi.

# TABLE OF CONTENTS

ACKNOWLEDGMENTS . . . . . iii
ACADEMIC ETHICS AND INTEGRITY STATEMENT . . . . . v
ABSTRACT . . . . . vi
ÖZET . . . . . vii
LIST OF FIGURES . . . . . xi
LIST OF TABLES . . . . . xiii
LIST OF SYMBOLS . . . . . xiv
LIST OF ABBREVIATIONS . . . . . xv
1. INTRODUCTION . . . . . 1
1.1 Botulinum Toxin Treatment . . . . . 1
1.2 Myofascial Force Transmission . . . . . 3
1.2.1 Isolated Muscle Level . . . . . 4
1.2.2 In vivo Muscle Level . . . . . 4
1.3 Motivation of the Thesis . . . . . 5
2. MECHANICAL PRINCIPLES OF EFFECTS OF BOTULINUM TOXIN ON MUSCLE LENGTH-FORCE CHARACTERISTICS: AN ASSESSMENT BY FINITE ELEMENT MODELING . . . . . 8
2.1 Methods . . . . . 10
2.1.1 Description of the model . . . . . 10
2.1.2 Models for the BTX-free muscle and several BTX-cases . . . . . 12
2.1.3 Solution procedure . . . . . 12
2.1.4 Processing of data . . . . . 13
2.2 Results . . . . . 14
2.2.1 Longer sarcomere effect . . . . . 14
2.2.2 Enhanced active force exertion . . . . . 15
2.2.3 $l_m$ dependence of $F_{reduction}$ . . . . . 15
3. INTACT MUSCLE COMPARTMENT EXPOSED TO BOTULINUM TOXIN TYPE A SHOWS COMPROMISED INTERMUSCULAR MECHANICAL INTERACTION . . . . . 18

3.1 Methods . . . 19
3.1.1 Animal models . . . 19
3.1.2 Surgical procedures . . . 20
3.1.3 Experimental Setup . . . 21
3.1.4 Experimental conditions and procedure . . . 22
3.1.5 Histological analysis of effects of BTX-A on intra- and epimuscular connective tissue content in combination . . . 24
3.1.6 Data Processing and Statistics . . . 25
3.2 Results . . . 27
3.2.1 Effects on TA and EHL . . . 27
3.2.1.1 Proximal forces . . . 28
3.2.1.2 Distal forces . . . 29
3.2.2 Proximo-distal active force differences . . . 30
3.2.3 Effects on intra- and epimuscular connective tissue content . . . 31
4. SIMULATION OF EFFECTS OF BOTULINUM TOXIN ON MUSCULAR MECHANICS IN DUE TREATMENT COURSE BASED ON ADVERSE EXTRACELLULAR MATRIX ADAPTATIONS CAUSING INCREASED STIFFNESS . . . 34
4.1 Methods . . . 35
4.1.1 Modeled BTX cases . . . 35
4.1.2 Description of the model . . . 35
4.1.3 Solution procedure . . . 39
4.1.4 Processing of data . . . 39
4.2 Results . . . 40
4.2.1 Longer/shorter sarcomere effect . . . 40
4.2.2 Enhanced active force production capacity . . . 41
4.2.3 Narrower active $l_{range}$ . . . 42
5. DISCUSSION . . . 44
5.1 Mechanisms of modeled effects of BTX in isolated muscle . . . 44
5.2 BTX-A causes diminished effects of EMFT and a position-dependent force reduction . . . 47
5.3 Time course of BTX treatment . . . 49

5.4 Implications and specific limitations of Animal experimentation . . . . 51
5.5 Muscle model limitations . . . . . 54
5.6 Future Directions . . . . . 58
5.7 Model Of Anterior Crural Compartment (ACC) Muscles With Epimuscular Connections . . . . . 58
5.7.1 TA Muscle Anatomy And Its Model . . . . . 60
5.8 Conclusion . . . . . 62
APPENDIX A. Description of the "Linked Fiber-Matrix Mesh model" . . . . 65
A.0.1 Extracellular Matrix Element . . . . . 66
A.0.2 Myofiber Element . . . . . 67
A.0.3 Aponeurosis Element . . . . . 69
A.0.4 Model of Isolated Intact EDL Muscle . . . . . 70
REFERENCES . . . . . 71

# LIST OF FIGURES


| | | |
|---|---|---|
| Figure 2.1 | Finite element modeling of EDL muscle. | 11 |
| Figure 2.2 | Schematic representation of modeled BTX-cases. | 13 |
| Figure 2.3 | Effects of BTX related partial activation on distribution of muscle fiber direction mean strain. | 16 |
| Figure 2.4 | Effects of BTX related partial muscle activation on muscle length force characteristics. | 17 |
| Figure 3.1 | Illustrations of the experimental setup and conditions. | 23 |
| Figure 3.2 | Forces of the TA and EHL muscles as a function of changing EDL relative muscle position. | 27 |
| Figure 3.3 | Forces of the EDL muscle as a function of changing EDL relative muscle position. | 28 |
| Figure 3.4 | EDL proximo-distal active force differences as a function of changing EDL relative muscle position. | 32 |
| Figure 3.5 | Sample histological sections of AC compartment stained using Gomori trichrome for collagen. | 33 |
| Figure 4.1 | Nonlinear and anisotropic material properties of the extracellular matrix element in the local coordinates. | 36 |
| Figure 4.2 | Finite element modeling of EDL muscle and partial paralysis. | 37 |
| Figure 4.3 | Simulated effects of different phases of BTX treatment on distribution of muscle fiber direction mean strain. | 41 |
| Figure 4.4 | Simulated effects of different phases of BTX treatment on distribution of muscle fiber direction mean stress. | 42 |
| Figure 4.5 | Simulated effects of different phases of BTX treatment on muscle length-force characteristics. | 43 |
| Figure 5.1 | Compartment model representation | 59 |
| Figure 5.2 | Lateral view of ACC compartment. | 61 |
| Figure 5.3 | Model representation of EDL and EHL | 62 |
| Figure 5.4 | The components of the neurovascular tract and its location. | 63 |

Figure A.1 Passive non-linear and anisotropic material properties of the extracellular matrix element in the local coordinates 67
Figure A.2 Active stress strain properties of the myofiber element representing the contractile apparatus 68
Figure A.3 Mechanical properties representing the titin filaments 69

# LIST OF TABLES

Table 5.1 Anterior Crural Compartment Muscles' Dimensions 59

# LIST OF SYMBOLS

| | |
|---|---|
| $l_m$ | Muscle length |
| $F_{reduction}$ | Force reduction |
| $l_{mo}$ | Optimum muscle length |
| $\Sigma\sigma_{active}$ | The summed nodal fiber direction stresses |
| $\Delta\Sigma\sigma_{active}$ | The difference between $\Sigma\sigma_{active}$ of a BTX-case and a BTX-free muscle |
| $F_{reduction-comp}$ | Compromise to force reduction |
| $\Delta posit_{EDL}$ | EDL muscle position change |
| $l_{range}$ | Muscle Length Range |

# LIST OF ABBREVIATIONS

| | |
|---|---|
| BTX | Botulinum Toxin |
| MFT | Myofascial Force Transmission |
| EDL | Extensor Digitorum Longus muscle |
| EHL | Extensor Hallucis Longus muscle |
| PHP | Proximal half paralyzed |
| MHP | Middle half paralyzed |
| DHP | Distal half paralyzed |
| CV | Coefficient of variation |
| MRI | Magnetic Resonance Imaging |
| ECM | extra-cellular matrix |
| LFMM model | Linked fiber mesh model |
| CP | Cerebral palsy |
| UMN | Upper motor neuron |
| LSE | Longer sarcomere effect |

# 1. INTRODUCTION

## 1.1 Botulinum Toxin Treatment

In disorders causing abnormal muscle activity, different therapies are applied depending on the clinical condition of the patient. In patients suffering from for example cerebral palsy, early intramuscular injection of Botulinum toxin type A (referred here as BTX) is effective in preventing contractures development [1] and musculoskeletal deformities [2]. In short, BTX is used to reduce the muscle activity and induce weakness (i.e., decreasing the ability for force exertion) of spastic muscle [3] by preventing the release of the primary neurotransmitter acetylcholine in the synapses [4]. The toxins ability to easily pass through muscle fascia [5] and specificity to motor neuron terminals [6] makes it ideal for muscle weakness formation. This muscle weakening property is at the center of clinical applications of BTX. As BTX has been utilized in many other clinical applications, its mechanical and non-mechanical secondary properties became increasingly important.

Many parameters are investigated to increase the effectiveness of BTX. However, as a direct measure of paralyzation, paralyzed muscle volume has been the primary focus. Studies showed that BTX does not paralyze the entire muscle [7], on the contrary creates a pattern of active and paralyzed fibers [8] [9]. Additionally in their work on injection location, Shaari and Sanders [9] reported that injections near the motor-end plate region maximized the paralyzed muscle volume and a deviation of only 0.5 cm from this region decreased the paralyzed muscle volume by 50 %. Also, increases in dose increased paralysis as expected however, the authors concluded that delivering toxin in small volumes near the motor end plate band of a muscle is most effective. This physiology-based study indicates that paralysis due to BTX generates paralyzed and non-paralyzed regions within the target muscle. Shaari et al. [5] investigated the diffusion of the toxin through the connective tissues of the muscle and revealed that the toxin blockage is limited. Yaraskavitch et al. [10] measured the length-force relationship

of the plantaris muscle of the cat after BTX injection to the neighboring soleus muscle and reported a significant force reduction up to 14 % although the muscle was not injected with the toxin. Our group had similar findings; length-force measurements on the muscles of intact rat anterior crural compartment showed that injection of BTX to the tibialis anterior muscle caused significant force decrease in all of the muscles of the compartment [11].

In addition to BTX-induced weakness studies described above, several studies revealed indirect or structural effects of BTX: E.g. BTX has been used as a tool to establish a controlled and reversible muscle weakness model for studying the effects of weakness on joint degeneration leading to osteoarthritis [12] [13]. Longino et al. [12] aimed to determine if BTX induced quadriceps weakness causes muscle dysfunction beyond that caused by anterior cruciate ligament transection in the knee by measuring isometric knee extensor torque, quadriceps muscle mass, and ground reaction forces. Similarly, Youssef et al. [13] studied the effects of BTX induced quadriceps weakness on microstructural changes in knee cartilage and reported that quadriceps muscle weakness caused increased degeneration in the retropatellar cartilage of rabbits, providing evidence that muscle weakness might be a risk factor for the onset and progression of osteoarthritis. Both studies used BTX to induce force decreases to show the effects of muscle weakness on pathologies. Another interesting study performed by Fortuna et al. [14] investigated structural changes such as muscle mass and contractile material in rabbits and reported less pronounced but similar results for non-targeted muscles, suggesting that repeated BTX injections cause muscle atrophy and loss of contractile tissue in target muscles and also in nontargeted muscles that are far removed from the injection site. However, these works on BTX application do not specifically addressed how the toxin affects the muscle mechanically.

Several studies addressed the mechanical effects of BTX using more direct approaches: In his experiment on rabbit knee extensors, Longino et al [15] showed that the paralyzing effects of BTX are not uniform. The muscle weakness is found to be greater at short compared to long muscle lengths and at low compared to high stimulation frequencies four weeks following intervention. Similarly, Yaraskavitch et al. [10]

studied forcelength properties of cat soleus muscle within and exceeding the functional range of motion at different frequencies of stimulation. BTX associated force loss was significantly different at all frequencies of stimulation and all lengths for the soleus. Note that measurements of muscle tension and the corresponding EMG evoked by stimulation of extra ocular muscle by Dimitrova et al. [16] showed similar frequency dependent decreases but no significant changes in muscle-speed-related characteristics. This result suggests an indiscriminant functional effect of BTX on all muscle fiber types. However, these results could be explained through a variety of mechanisms and therefore remain unclear or incomplete. Yaraskavitch et al. [10] proposed that the observed nontargeted muscle weakness across the long muscle lengths is the result of toxin leakage to surrounding muscles, while Fortuna et al. [14] discussed on possible effect of atrophy caused by muscle disuse as an alternative to direct relation to BTX. Yet, none of these studies have specific mechanical data and therefore remain limited to physiological reasoning.

## 1.2 Myofascial Force Transmission

In classical point of view of force transmission, muscle force generated by the fibers is transmitted to the tendon and from there onto the bones to cause movement. In biomechanics, particularly in modeling approaches, generally this Myotendinous Force Transmission path is assumed to be the exclusive channel. The connections between adjacent fibers, transsarcolammel connections of myofibers to the extracellular matrix [17] are not assumed to have mechanical significance and ability to transmit force (e.g., [18]). As a result serial and parallel sarcomere length heterogeneity were considered non-existent and in treatment of muscle-based pathologies, length of a single sarcomere was representative of the whole fiber or even muscle (e.g., [19]).

### 1.2.1 Isolated Muscle Level

As opposed to classical point of view, the connective tissue was shown to transmit force in single fiber [20], fiber bundles [21, 22], with experiments on isolated in-situ muscle [23, 24, 25, 26], and finite element models [27]. Such Force Transmission is called Intramuscular Myofascial Force transmission. Accordingly, mechanical interactions are not limited to sarcomeres in a fiber but also happen between the sarcomeres of neighboring fibers. As a result of this intramuscular Myofascial force transmission, sarcomere lengths may vary locally and throughout the muscle. The shift of muscle optimum length to higher length [28, 29] and consequently an increase in the joint range of motion are the important functional outcomes of inhomogeneous sarcomere length distributions [30]. Additionally, both parallel and in series sarcomere length distribution is the determinant of force produced at different muscle lengths.

### 1.2.2 In vivo Muscle Level

In vivo, a muscle is not isolated: (1) neighboring muscles have direct connections and recent animal experiment [31, 32, 33, 34] and in vivo human MRI studies [35] showed myofascial force transmission also occurs with neighboring the muscles: intermuscular myofascial force transmission. (2) Additionally, physiologically functional structures such as veins and neurons that innervate the muscle are covered with collagen-based structure. This structure is continued through structures such as septum, membranes and bones that are shown to transmit force [31, 36, 34]: extramuscular myofascial force transmission. The integrated structure composed of inter- and extramuscular connections is defined as epimuscular connections [33].

The effects of these epimuscular connections shown in previous studies are proximo-distal force differences [31, 29], more heterogeneous sarcomere length distribution [37, 38], increased length range of active force exertion [34].

## 1.3 Motivation of the Thesis

Literature studies so far do not offer specific methods or ask specific questions for determining mechanical mechanism of BTX. In this thesis, an understanding to the mechanical mechanisms of BTX treatment is provided both experimentally and computationally. A time line to these mechanical effects are established.

Sarcomere length change distribution is the main determinant of muscle force. However, sarcomere length distribution cannot be obtained experimentally. Therefore, if the mechanical mechanisms pertaining muscle force changes are of concern as in BTX application, methods with appropriate approaches should be adopted. At this point, previously developed [27] and experimentally validated (e.g., [29, 34]) finite element model that has contributed to understanding basic muscle mechanics (e.g., [33, 11, 29, 39]) has been modified for a finer mesh and therefore higher resolution. Hereby, it provided a reliable method to identify the mechanical mechanism in BTX application. Mechanical parameters such as sarcomere length distribution, proximo-distal force differences and normalized stress distributions were used. Note that the recently acknowledged Myofascial Force Transmission concept explained above plays an important role in determining the epimuscular mechanical mechanism of BTX application. Specific hypotheses and aims in this thesis are:

(i) to show the intramuscular mechanism of partial paralyzation created by BTX using finite element modeling. It is hypothesized that intramuscular interactions, i.e. intramuscular myofascial force transmission, will be central to length dependent force reduction effect of BTX shown experimentally.

(ii) to determine how epimuscular myofascial force transmission is affected from BTX application in vivo using animal experiment. It is hypothesized that epimuscular interactions diminish due to BTX application and intramuscular adaptations in the form of collagen material change occur.

(iii) to shown functional and mechanical time course of BTX computationally.

It is hypothesized that adaptations found experimentally would further enhance effects found on isolated muscle model and if such adaptations were to remain post-treatment, mechanical mechanism of the muscle would be altered permanently.

With the progression of aims from acute intramuscular effects to the effects of the treatment at full time course, a complete narration of the treatments mechanical effects are aimed to achieve. While computational modeling gives valuable information on mechanical mechanisms, animal experiments showed cumulative in-vivo effects that steered the research to focusing intramuscular effects, providing an essential information: BTX treatment diminishes epimuscular myofascial force transmission. Summaries of the chapters based on these hypotheses and consisting of published/submitted papers are as follows:

Chapter 2 Turkoglu, A.N., Huijing, P.A., Yucesoy, C.A., 2014. Mechanical principles of effects of botulinum toxin on muscle length-force characteristics: An assessment by finite element modeling. Journal of Biomechanics 47, 1565-1571. Modeling of partially paralyzed isolated muscle showed that force reduction originating exclusively from the paralyzed muscle fiber populations, is compromised by the changes of active sarcomeres leading to a smaller net force reduction. Moreover, such compromise to force reduction varies as a function of muscle length and is a key determinant of muscle length dependence of force reduction caused by BTX. Due to longer sarcomere effect, muscle optimum length tends to shift to a lower muscle length. Muscle fiber-extracellular matrix interactions occurring via their mutual connections along full peripheral fiber lengths (i.e., myofascial force transmission) are central to these effects.

Chapter 3 Yucesoy, C.A., Turkoglu, A.N., Umur, S., Ates, F., 2015. Intact muscle compartment exposed to botulinum toxin type a shows compromised intermuscular mechanical interaction. Muscle Nerve 51, 106-116. The forces of the anterior crural compartment muscles (The tibialis anterior (TA), extensor hallucis longus (EHL) and extensor digitorum longus (EDL)) were measured in Wistar rats. Two groups of Wistar rats were tested: Control (no BTX-A injected) and BTX (0.1 units of BTX-A injected into the mid-belly of TA). TA and extensor EHL muscles were kept at con-

stant length, whereas the position of the extensor digitorum longus (EDL) muscle was changed exclusively. The results showed that Epimuscular Myofascial Force Transmission is diminished. Another important finding was the decrease in the percentage of intra- and epimuscular connective tissue content values for the BTX group.

Chapter 4 Turkoglu Ahu N. and Yucesoy Can A. 2015 Simulation of effects of botulinum toxin on muscular mechanics in due treatment course based on adverse extracellular matrix adaptations causing increased stiffness Submitted to Journal of Biomechanics Modeling study in chapter 2 showed that partial muscle paralyzation per se causes restricted sarcomere shortening which enhanced potential of active force production and decreased muscle length range of force exertion. Moreover, experimental results in chapter 3 indicated also increased Extracellular Matrix stiffness of BTX treated muscle. Hence, altered muscle fiber-ECM interactions and BTX effects are plausible in due treatment course. In this chapter, the change in the mechanical mechanism of BTX treatment is studied using finite element modeling. Model results showed that with increasing ECM stiffness sarcomere shortening effect gets more pronounced in the long-term and is persistent or reversed (longer muscle lengths) post-BTX treatment. Consequently, force production capacity of activated sarcomeres gets further enhanced in the long-term. Post-treatment, remarkably, such enhanced capacity becomes permanent for the entire muscle. Shift of muscle optimum length to a shorter length is more pronounced in the long-term and some of which remains permanent post-treatment.

# 2. MECHANICAL PRINCIPLES OF EFFECTS OF BOTULINUM TOXIN ON MUSCLE LENGTH-FORCE CHARACTERISTICS: AN ASSESSMENT BY FINITE ELEMENT MODELING

Muscle spasticity is characterized by an imbalance in the excitatory and inhibitory modulation of neuromuscular reflex loops, leading to a velocity-dependent increase in stretch-reflex activity (e.g., [40], hypertonia [41, 42] and an increase in muscle resistance to passive stretch [43]. Early intramuscular injection of botulinum toxin (BTX) aims at temporary reduction in spasticity by chemodenervation and by causing decreased afferent discharges [44, 45, 46].

BTX has been reported also to be effective in preventing development of contractures [1] and musculoskeletal deformities [2]. Clinically relevant practical aspects of BTX treatment (e.g., intramuscular injection site and dose) have been addressed [6, 9], and effects regarding reduction of spasticity [47, 48], and improved joint movement [49, 50] have been reported.

However, reduction of spasticity is not the exclusive effect, as BTX treatment causes a partial muscle paralysis [7, 9]. Therefore, one aspect of its effects is decreased ability for force exertion of BTX-treated muscle. In animal experiments (e.g., [51, 12, 11] such effects were shown to occur. Yet, views on clinical consequences of force reduction ($F_{reduction}$) are still controversial. An imbalance of agonistic and antagonistic muscle forces acting at a joint is considered to cause a decreased joint range of motion hence an impeded function, and reducing the force of the spastic muscle is considered to counteract such imbalance (e.g., [52]). However, spastic muscle is also considered as not strong enough and further $F_{reduction}$ is not regarded as an indicated therapeutic effect (e.g., [53]). Nevertheless, skeletal muscle is still the actuator of movement. Therefore, a comprehensive understanding of effects of BTX on muscular mechanics is crucial.

Despite many studies on global effects of BTX, such understanding has not been attained. Possible explanations for that are: (1) most reports regarding twitch and tetanic force have been limited to selected muscle lengths ($l_m$) or joint positions [54, 16], with an implicit assumption that $F_{reduction}$ is not variable with $l_m$. However, muscle length-force curves (l-F curves, being a collection of muscle force data measured at several isometric muscle lengths) show that such $F_{reduction}$ becomes gradually less pronounced with increasing $l_m$ [10, 11]. Moreover, recent experiments involving such measurements of muscle forces at various lengths show that the length range of active force exertion (i.e., the length range between muscle active slack length and muscle optimum length) of a BTX-treated muscle is reduced [55]. These findings suggest that mechanical effects of BTX are more complex than a simple $F_{reduction}$. (2) Mechanisms of how secondary effects of BTX may change intramuscular mechanics are not well understood. $l_m$ dependent effects indicate that BTX may change physiological conditions of sarcomeres (particularly their lengths).

Intra- and extra-cellular domains of muscle fibers interact mechanically due to myofascial force transmission (MFT) [25, 56]. MFT has been defined as transmission of force between muscle fibers and their collagen fiber reinforced extra-cellular matrix (ECM) via macromolecular connections along the full length of the muscle fibers [17, 57, 58]. Evidence for muscle fiber-ECM interactions was shown experimentally for single muscle fibers [20], for isolated bundles of muscle fibers [21] and whole dissected muscle [23]. Therefore, the length of a sarcomere is not determined exclusively by its interaction with sarcomeres arranged in series within the same fiber, but also by forces exerted on it by the ECM and sarcomeres of neighboring muscle fibers.

Finite element modeling showed that changes of muscle fiber-ECM interactions imposed by manipulating the stiffness of connections between them [27] or by creating a discontinuity within the ECM [30] alter the force balance determining sarcomere length and hence affect mechanical contributions of sarcomeres to muscle l-F curves. BTXinduced partial-paralysis changes intramuscular MFT. We hypothesize that such changes affect conditions of sarcomeres within active parts of the muscle and that this plays a role in determining $l_m$ dependent effects of BTX. Using finite element modeling,

our goal was to test this hypothesis and to study principles of how such partial-paralysis per se affects muscle mechanics.

## 2.1 Methods

### 2.1.1 Description of the model

Using a two-domain approach, a 3D-finite element muscle model (linked fiber-matrix mesh model: LFMM model) was developed [27]. This model consists of two meshes, occupying the same space, that are linked elastically. These meshes represent the ECM domain (matrix mesh) and intracellular domain (fiber mesh). Such modeling allows assessment of effects of muscle fiber-ECM interactions.

The two meshes are built using the self-programmed myofiber and ECM elements that were introduced as user defined elements into a finite-element analysis software (ANSYS Academic Teaching Advanced v.12.0 ANSYS. Inc. Canonsburg, PA, USA). The elements have eight nodes and linear interpolation functions. The tissues are considered as a continuum and a large deformation analysis is employed. A 3D local coordinate system representing the fiber, cross-fiber, and thickness directions is used. For the myofiber element, the total stress acting only in the fiber direction equals the sum of the active stress of the contractile elements (representing active force exertion based on overlap of actin and myosin myofilaments) and the stress due to intracellular passive tension (originating from the intra-sarcomeric cytoskeleton, with a dominant role played by titin). It is assumed that the sarcomeres arranged in-series within muscle fibers have identical material properties. The ECM element incorporates a strain energy density function that accounts for the non-linear and anisotropic material properties and the constancy of muscle volume. For full details including description of constitutive relationships, model parameters and activation procedure, see a review by Yucesoy and Huijing [11].

One muscle element (a linked system of ECM and myofiber elements) is defined

to represent a segment of a bundle of muscle fibers, its connective tissues and the links between them.

In the LFMM model, both matrix and fiber meshes are rigidly connected to single layers of standard hyperelastic elements (ANSYS element library: HYPER58 elements) forming the muscles proximal and distal aponeuroses. Standard spring elements (ANSYS element library: COMBIN39 elements) are used to represent the transmembranous attachments i.e., the elastic links between the two meshes. This is a 2-node spring element, set to be uni-axial and having linear high stiffness representing non-pathological connections between the muscle fibers and the ECM (for an analysis of the effects of stiff or compliant links, see [27]). Initially, these links have zero length.

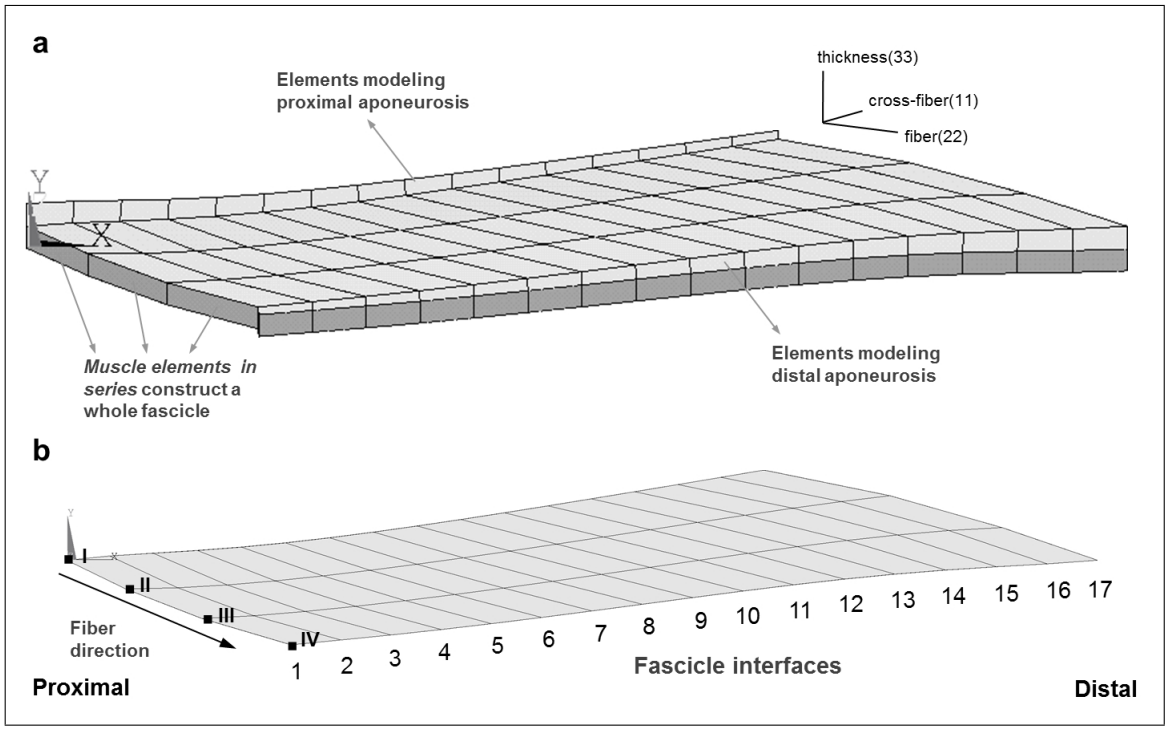



**Figure 2.1** Finite element modeling of EDL muscle. (a) The model consists of three muscle elements in series and sixteen in parallel. Each combination of three muscle elements arranged in series constructs a whole fascicle. The muscle elements located proximally and distally are connected to elements representing the muscles aponeuroses. A 3D local coordinate system representing the fiber, cross-fiber (normal to the fiber direction), and thickness directions is used for the analysis and presentation of the model results. (b) A combination of nodes along one side of a fascicle is referred to as a fascicle interface. For example, the most proximal fascicle interface is a combination of the four nodes indicated by a Roman numeral from I to IV. Each fascicle interface is indicated from by a number from 1 to17.

### 2.1.2 Models for the BTX-free muscle and several BTX-cases

To represent all cases studied, the extensor digitorum longus (EDL) muscle of the rat was modeled. This muscle is unipennate with a minimal variation of its muscle fiber directions. The geometry of the model (Figure 2.1a) is defined as the contour of a mid-longitudinal slice of the EDL muscle belly. A whole fascicle is constructed by putting three muscle elements in series. Sixteen of those are arranged in parallel, filling the slice space. A combination of nodes along one side of a fascicle is referred to as a fascicle interface (Figure 2.1b).

BTX-free muscle was modeled by activating maximally all myofiber elements. BTX-treated muscle was modeled by activating only selected fascicles within the muscle, leaving the remainder inactive. This allows studying principles of mechanisms of isolated effects of BTX on muscular mechanics. A BTX-case refers to the whole muscle volume including inactivated muscle parts, as well as activated muscle parts. Three BTX-cases were considered (Figure 2.2a) each of which having an identical number of inactivated muscle fascicles (i.e., a similar muscle volume paralyzed): (I) proximal half (fascicles 1-8) paralyzed (PHP), (II) middle half (fascicles 5-12) paralyzed (MHP) and (III) distal half (fascicles 9-16) paralyzed (DHP).

### 2.1.3 Solution procedure

At the initial $l_m$ (28.7 mm), and in the passive state, the serial sarcomeres within muscle fibers were assumed to be in the undeformed state (i.e., strain equals zero, and sarcomere length approximates 2.5). Local fiber strain, as a measure of change of length, reflects lengthening (positive strain) or shortening (negative strain) of sarcomeres.

Static analysis was performed, using a force-based convergence criterion (tolerance=0.5%). Muscle origin was fixed whereas, after activation, the position of the insertion was changed to new isometric lengths.

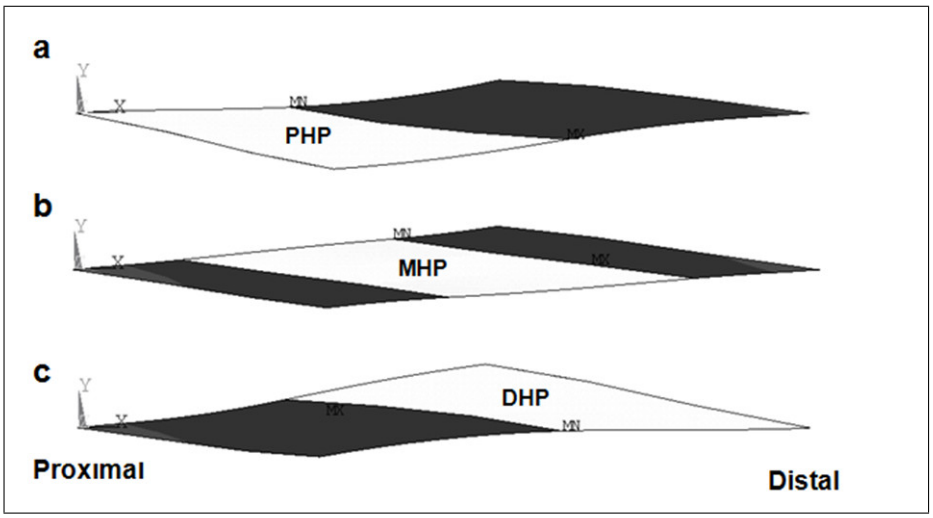



**Figure 2.2** Schematic representation of modeled BTX-cases. Typical deformed shape after distal lengthening of BTX-cases modeled by not activating muscle elements located in (a) the proximal half (PHP), (b) the middle half (MHP) and (c) the distal half (DHP) of the muscle: white areas within the muscle belly indicate paralyzed muscle parts whereas, the darker areas indicate the parts that are activated maximally.

### 2.1.4 Processing of data

l-F curves were studied to quantify $F_{reduction}$. All forces are normalized for the maximal total force of BTX-free muscle.

The mean nodal fiber direction strain per fascicle interface is considered to represent sarcomere length changes in BTX-cases vs. BTX-free muscle.

Within the physiological context, muscle optimum length ($l_{mo}$) corresponds to the length at which, on average, active sarcomeres attain their optimum length. For each BTX-case, $l_{mo}$ is determined considering only the activated muscle parts: using a least squares approach, $l_m$ at which mean nodal fiber direction strains of active fascicle interfaces is closest to zero is determined to represent $l_{mo}$. $l_{mo}$ of BTX-cases are compared to that of BTX-free muscle.

The summed nodal fiber direction stresses for fascicle interfaces of the activated muscle parts ($\Sigma\sigma_{active}$) represent an index for the potential of active force exertion for BTX-cases. $\Sigma\sigma_{active}$ values of BTX-cases are compared to the matching value of the

BTX-free muscle: i.e., the particular nodes of the BTX-free muscle corresponding to those within the activated muscle parts of a particular BTX-case were used exclusively to calculate $\Sigma\sigma_{active}$. $\Delta\Sigma\sigma_{active}$ is calculated as the difference between $\Sigma\sigma_{active}$ calculated for a BTX-case and that for the BTX-free muscle. For a BTX-case, a greater $\Delta\Sigma\sigma_{active}$ indicates enhanced active force exertion with respect to the same selection of sarcomeres within the BTX-free muscle.

$l_m$ range studied includes lengths between a short ($l_m = 25.2$ mm) and a long length ($l_m = 30.7$ mm). Mean fiber direction strains are assessed at those lengths and at an intermediate one ($l_m = 29.0$ mm).

## 2.2 Results

### 2.2.1 Longer sarcomere effect

Except for a few fascicle interfaces (at $l_m = 25.2$ mm), mean fiber direction strain curves for BTX-free muscle are localized below those of the BTX-cases (Figure 2.3). This means that sarcomeres throughout the BTX-muscle attain higher lengths: (1) the inactivated fascicles in BTX-cases, do not shorten as much as their activated counterparts within the BTX-free muscle (e.g., at $l_m = 25.2$ mm, the inactivated fascicles of case MHP and the same parts within BTX-free muscle shortened by 29-27% and 32-29%, respectively (Figure 2.3b)). (2) Despite maximal activation, most active sarcomeres (i.e. also those located in the activated parts of the BTX-cases) were longer than their counterparts within BTX-free muscle (e.g., at $l_m = 30.7$ mm, the activated fascicles of case MHP and the same parts of the BTX-free muscle are lengthened by 9-13% and 3-12%, respectively (Figure 2.3c)). Therefore, for all $l_m$, a vast majority of sarcomeres are at higher lengths than sarcomeres of the BTX-free muscle. We will refer to this effect as longer sarcomere effect (LSE), which implies: BTX-case sarcomeres active at the ascending limb of their l-F curve should exert more force compared to their counterparts in BTX-free muscle and opposite effect for sarcomeres at the descending limb.

As a consequence of LSE, $l_{mo}$ for BTX-free muscle (30.1mm) shifts to a lower length in BTX-cases (29.7, 29.5 and 29.3 mm respectively for cases PHP, DHP and MHP).

### 2.2.2 Enhanced active force exertion

$\Sigma\sigma_{active}$ for BTX-cases is enhanced (up to 14.5%) compared to corresponding parts of BTX-free muscle (Figure 2.4a). Therefore, remarkably the activated parts of the BTX-cases produce more active force, which compromises $F_{reduction}$ ($F_{reduction-comp}$).

### 2.2.3 $l_m$ dependence of $F_{reduction}$

Both $\Sigma\sigma_{active}$ (as an estimate of $F_{reduction-comp}$, Figure 2.4a) and $F_{reduction}$ (Figure 2.4b) are a function of $l_m$. For example case DHP (see critical muscle lengths marked as x, y and z in Figure 2.1a b). Initially, $F_{reduction-comp}$ attains a low value and $F_{reduction}$ peaks (x). With increasing $l_m$, $F_{reduction-comp}$ increases until reaching a maximum (y). With further increased lengths, $F_{reduction-comp}$ continuously decreases (below z). $F_{reduction}$ decreases with increasing lengths however, between x and y, this decrease is steep and beyond y more gradual. Case PHP shows a similar effect. Therefore, a key determinant is how much $F_{reduction}$ is compromised by LSE as this effect causes the $l_m$ dependence of actual $F_{reduction}$.

This is consistent also for case MHP: Below $l_m = 29.6$ mm, the greatest $F_{reduction-comp}$ and hence the lowest $F_{reduction}$, over that length, the lowest $F_{reduction-comp}$ and hence the biggest $F_{reduction}$ are found.

Modeled l-F curves are shown in Figure 2.4c.

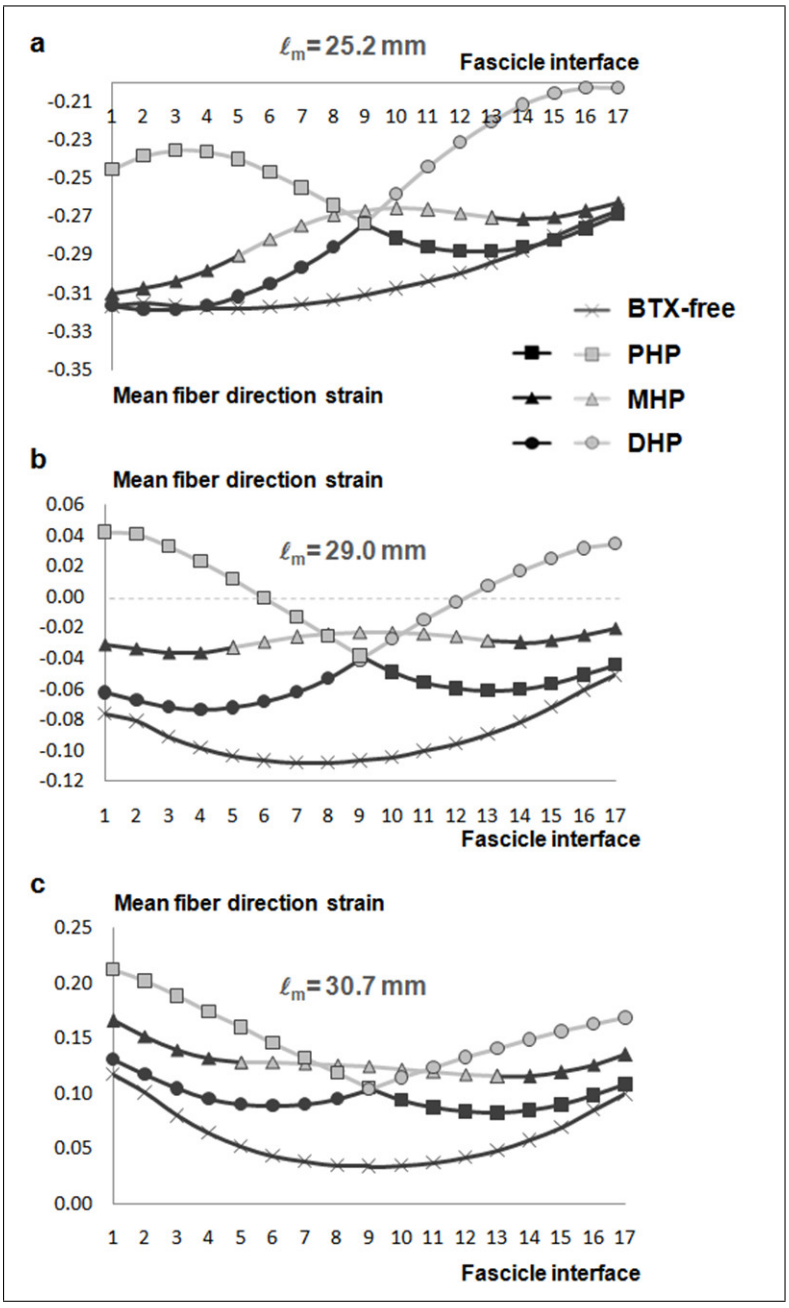



**Figure 2.3** Effects of BTX related partial activation on distribution of muscle fiber direction mean strain. In the strain plots activated (dark lines and dark bullets) and paralyzed (lighter lines with lighter bullet filling) muscle parts are distinguished. Muscle lengths considered are (a) $l_m = 25.2$ mm , (b) $l_m = 29.0$ mm, and (c) $l_m = 30.7$ mm. Mean strain distributions are shown for BTX-free muscle, as well as BTX-cases, proximal half paralyzed muscle (PHP), middle half paralyzed muscle (MHP) and distal half paralyzed muscle (DHP). Activated muscle parts: fascicles 9-17 for case PHP, fascicles 1-5 13-17 for case MHP and fascicles 1-9 for case DHP. Paralyzed muscle parts: fascicles 1-9 for case PHP, fascicles 5-13 for case MHP and fascicles 9-17 for case DHP.

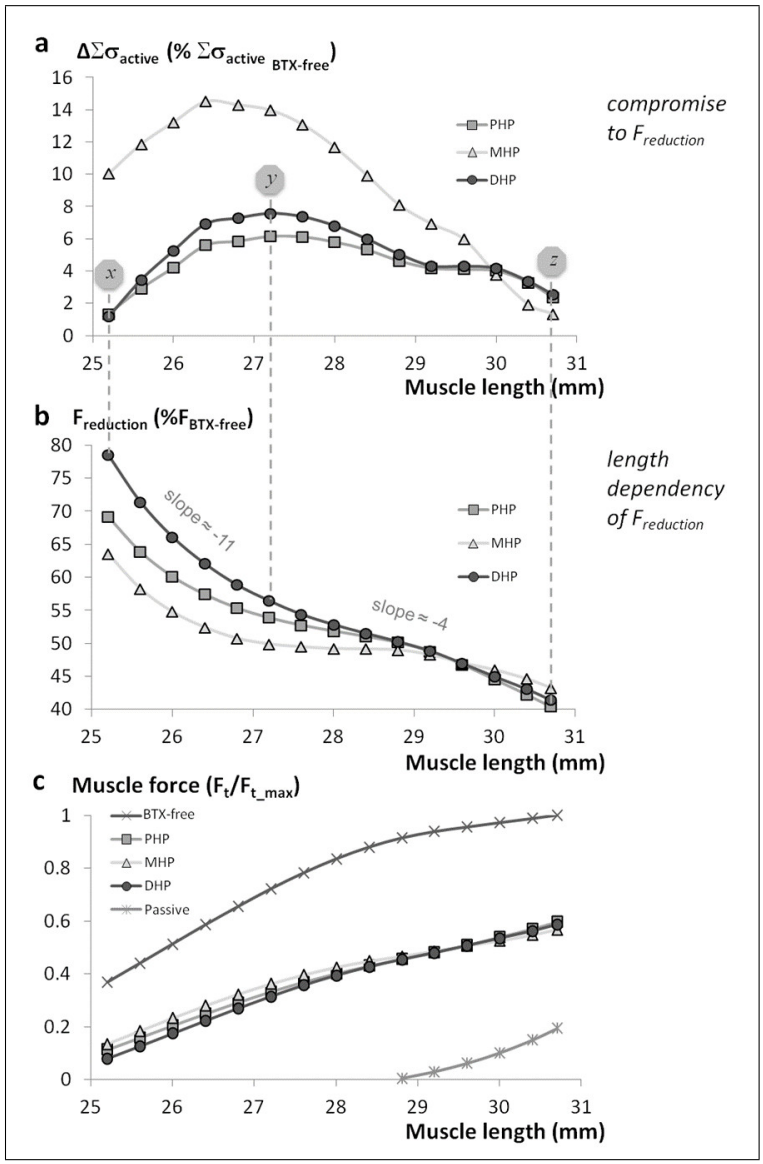



**Figure 2.4** Effects of BTX related partial muscle activation on muscle length force characteristics. (a) As an estimate of compromised force reduction ($F_{reduction-comp}$), $\Sigma\sigma_{active}$ (i.e., the difference between the summed nodal fiber direction stresses calculated for the activated muscle parts of the BTX-cases and the corresponding parts of the BTX-free muscle) is shown as a percentage of $\Sigma\sigma_{active}$ of the particular BTX-case. The values ranging from 1.8% to 14.5% for different muscle lengths indicate that the activated muscle parts of the BTX-cases can produce more force than the corresponding parts within the BTX-free muscle. (b) Length dependence of $F_{reduction}$. Percent decreases in muscle active force for BTX-cases are shown as a function of muscle length. In (a) and (b) critical muscle lengths for Case DHP are indicated to exemplify how $F_{reduction-comp}$ is related to $F_{reduction}$ with changing $l_m$. x marks $l_m = 25.2$ mm, indicating the peak $F_{reduction}$ (78.6%) at the lowest muscle length. y marks $l_m = 27.2$ mm, indicating the peak $F_{reduction-comp}$ (6.2%). z marks $l_m = 30.7$ mm, indicating the minimum $F_{reduction}$ (41.4%) at the highest length. Between x and y where $F_{reduction-comp}$ increases, there is a much faster $F_{reduction}$ than between y and z where $F_{reduction-comp}$ decreases (compare slopes indicated in (b)).(c) The isometric muscle length force curves for the muscles modeled. Isometric total and passive force curves of BTX-free muscle as well as BTX-cases PHP, MHP and DHP are shown as a function of muscle length. All sets of data are normalized for studied maximal total force of BTX-free muscle.

# 3. INTACT MUSCLE COMPARTMENT EXPOSED TO BOTULINUM TOXIN TYPE A SHOWS COMPROMISED INTERMUSCULAR MECHANICAL INTERACTION

For muscles operating within an intact compartment, changes in their position relative to each other have been shown to be a co-determinant of muscle force in addition to muscle length [59, 36, 56]. Muscle epimuscular connections, include direct collagenous connections between neighboring muscles and neurovascular tracts and compartmental boundaries (for pictures, see [60, 30]). Relative muscle position changes cause muscle epimuscular connections to stretch, and myofascial loads acting on the muscle to build up. These loads may manipulate muscle force generation potential [29] and cause unequal forces to be exerted proximally and distally [31], as characteristic effects of epimuscular myofascial force transmission (EMFT) [61, 33].

Effects of EMFT have been shown in vivo [62, 63, 64, 65] and have been considered to play an important role in the mechanics of muscle in health [56]. Moreover, its potential important role in muscle spasticity has been addressed [66, 30]. EMFT imposes an abnormal mechanical interaction between simultaneously activated muscles leading to parallelism between mechanics of spastic muscle and joint movement disorder. A recent study supports this view point; it showed that spastic muscle tested intra-operatively has no abnormal muscle force-joint angle relationship, if it is activated alone [67]. EMFT also has effects in several types of remedial surgery employed for treatment of muscle spasticity [30]. For example, the mechanical mechanism of muscle lengthening surgery [38] is affected by EMFT in a major way [68, 69] such that, such force transmission causes asymmetrical effects at the proximal and distal tendons of the altered muscle and changes the forces of even non-treated synergistic muscles [70].

Botulinum toxin type A (BTX-A) is used widely for treatment of spasticity. It inhibits acetylcholine release into the presynaptic cleft in the neuromuscular junction and causes muscle weakness or paralysis [4, 71], decreased muscle tone [49, 50] and al-

tered sensory input [44, 46]. Consequently, both motor and sensory actions of BTX-A contribute to reduction of spasticity in, for example, cerebral palsy (CP) patients. However, the effects of BTX-A on muscular mechanics are much more involved than just muscle weakness. (1) BTX-A decreases the force of the muscles in the same compartment [11] due to spread of toxin [72, 73, 5]. (2) In studies in which muscle length-force relationships of control and BTX-A animal groups are compared, the reduction in muscle force due to BTX-A becomes less pronounced at higher muscle lengths, indicating that this effect is muscle length-dependent instead of constant [67, 10, 11]. (3) BTX-A exposure may change the range from muscle active slack length (the shortest length at which the muscle can still exert nonzero force) to muscle optimum length (the length at which the muscle force is maximum) [67].

However, length changes of muscles exposed to BTX-A were observed to affect the force of other muscles to only a limited extent [67, 11]. This is in contrast to the substantial effects of EMFT shown previously on the mechanics of untreated and surgically treated muscle ((for a review of several studies see [61, 30]). Therefore, another as-yet unidentified component to the effects of BTX-A on muscular mechanics could be compromised intermuscular mechanical interactions. Considering the potential importance of such interaction in spasticity, we tested the following hypothesis: BTX-A causes EMFT within a muscle compartment to become diminished. Experimentally changing the relative position of a muscle exclusively eliminates the effects of muscle length changes and allows the assessment of the effects of EMFT in isolation. We used this to test our hypothesis.

## 3.1 Methods

### 3.1.1 Animal models

Surgical and experimental procedures were approved by the Committee on the Ethics of Animal Experimentation at Boğaziçi University, Istanbul, Turkey. Male Wistar rats were divided into 2 groups: (1) Control (n=7, mean±SD body mass=302.2±4.2g).

(2) BTX-A (n=7, mean±SD body mass=313.0±4.4g).

After imposing mild sedation with a 1 mg/kg intraperitonal dose of ketamine, a circular region of approximately 15mm radius from the center of the patella was shaved in the left hind limb. The tibialis anterior (TA) muscle was located by palpation when the ankle was in maximal plantar flexion and the knee angle approximated 90°. After marking the center of the patella, a second marker was placed at a point 10mm distally along the tibia. The injection location was 5mm lateral (along the direction normal to the line segment drawn between the 2 markers) to the second marker and over the TA muscle. All injections were made exclusively into this muscle, to a depth of 3mm.

For the BTX-A group, each 100 unit vial of vacuum dried, Botulinum type A, neurotoxin complex (BOTOX, Allergan Pharmaceuticals, Westport, Ireland) was reconstituted with 0.9% sodium chloride. The animals received a one-time intramuscular BTX-A injection at a total dose of 0.1 units. The injected volume equaled 20 . The control group was injected with the same volume of 0.9% saline solution. All injections were performed 5 days prior to testing. The animals were kept separately until the day of the experiment in standard cages in a thermally regulated animal care room with a 12h dark-light cycle.

### 3.1.2 Surgical procedures

The animals were anesthetized using intraperitoneally injected urethane (1.2ml of 12.5% urethane solution/100g body mass). Additional doses were given if necessary (maximum, 0.5ml). Immediately following the experiments, the animals were euthanized by administration of an overdose of urethane solution.

During the surgery and data collection, the animals were kept on a heated pad (Homoeothermic Blanket Control Unit; Harvard Apparatus, Holliston, Massachusetts) to prevent hypothermia. A feedback system utilizing an integrated rectal thermometer allowed control of body temperature at 37°C by adjusting the temperature of the heated

pad.

The skin and the biceps femoris muscle of the left hind limb were removed, and the anterior crural (AC) compartment, including the extensor digitorum longus (EDL), the TA, and the extensor hallucis longus (EHL) muscles, was exposed. However, the compartment was left intact; only a limited distal fasciotomy was performed to remove the retinaculae (i.e., the transverse crural ligament and the crural cruciate ligament), and the connective tissues at the muscle bellies within the anterior crural compartment were not altered.

The specific combination of knee joint and ankle angles (120° and 100°, respectively) was selected as the reference position. In the reference position, the 4 distal tendons of the EDL muscle were tied together using silk thread. Matching markers were placed on the distal tendons of the EDL, the TA, and the EHL, as well as on a fixed location on the lower leg. Subsequently, the distal EDL tendon complex and the TA and the EHL tendons were cut as distally as possible. The proximal EDL tendon was cut from the femur, with a small piece of the lateral femoral condyle still attached. In order to provide connection to force transducers, Kevlar threads were sutured to: (1) the proximal tendon of the EDL muscle, (2) the tied distal tendons of the EDL muscle, (3) the distal tendon of the TA muscle, and (4) the distal tendon of the EHL muscle.

Within the femoral compartment, the sciatic nerve was dissected free of other tissues, during which process all nerve branches to the muscles of that compartment were cut. Subsequently, the sciatic nerve was cut as far proximal as possible.

### 3.1.3 Experimental Setup

The animal was mounted in the experimental set-up (Figure 3.1). The femur and foot were fixed with metal clamps with the ankle in maximum plantar flexion (180°) to allow for free passage of the Kevlar threads to the distal force transducers.

The knee angle was set at 120°. Each Kevlar thread was connected to a separate force transducer (FT) (BLH Electronics Inc., Canton, Massachusetts). Care was taken to ensure that the alignment of the Kevlar threads was in the muscle line of pull. The distal end of the sciatic nerve was placed on a bipolar silver electrode.

### 3.1.4 Experimental conditions and procedure

Room temperature was kept at 26°C. For the duration of the experiment, muscle and tendon tissues were irrigated regularly with isotonic saline to prevent dehydration. The distal FTs of the TA and EHL were kept at the reference position at all times (i.e., their muscletendon complex length was constant).

All muscles studied were activated maximally by supramaximal stimulation of the sciatic nerve (STMISOC; BIOPAC Systems, Goleta, California), using a constant current of 2mA (square pulse width 0.1ms). After setting the EDL muscle to a target length, 2 twitches were evoked, and 300ms after the second twitch, the muscles were tetanized (pulse train 400ms, frequency 100Hz). At 200ms after the tetanic contraction, another twitch was evoked. After each application of this stimulation protocol, the muscles were allowed to recover for 2 minutes.

*Prior to muscle position testing* EDL force-length characteristics were determined with the proximal FT kept in reference position. Starting from active slack length (i.e., the shortest length at which non-zero active force is exerted), EDL length was increased by moving its distal FT (in 1mm increments), until it was 2mm over the length at which the highest EDL active force was measured ($l_{mopt}$). Based on the data, 2 EDL lengths were distinguished: (1) $l_{mopt}$, referred to as high length and (2) 6mm below $l_{mopt}$, referred to as low length.

*Muscle position testing* In separate tests performed at high and low lengths, the effects of EDL position changes were studied. Target EDL length was set as described above by changing distal FT position distally, when the proximal FT was at reference

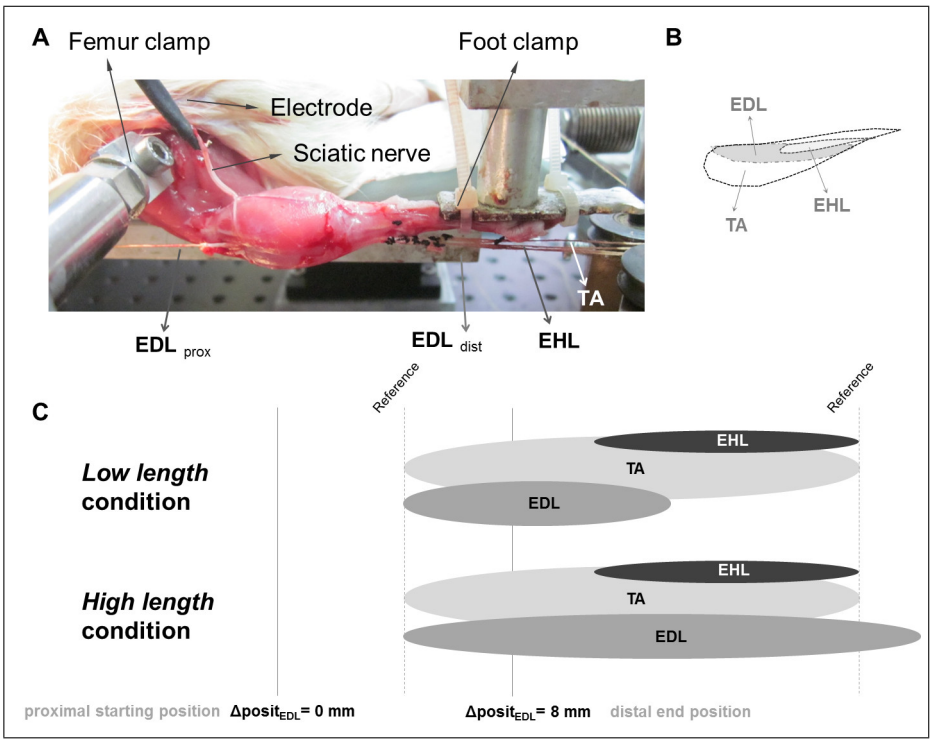



**Figure 3.1** Illustrations of the experimental setup and conditions. (A) The proximal ($EDL_{prox}$) and tied distal tendons of the EDL ($EDL_{dist}$), and the distal tendons of the tibialis anterior (TA) and extensor hallucis longus (EHL) muscles were each connected to a separate force transducer (FT) for simultaneous force measurements. Throughout the experiment, the TA and the EHL were kept at constant muscle-tendon complex lengths. Experimental condition: knee angle=120° with the ankle at maximum plantar flexion. The femur and the foot were fixed with metal clamps. The distal end of the sciatic nerve was placed on an electrode. Kevlar threads sutured to tendons provided connection to FTs (for more explicit illustrations see [67, 11]). (B) Relative sizes and locations of anterior crural muscles. (C) Schematics of studied muscle positions. With its proximal tendon at reference position, the EDL was brought to 6 mm below $l_m$ opt (low length) or to lm opt (high length). Its position was changed first by moving both of its FTs by 5mm proximally. From this proximal starting position ($\Delta posit_{EDL}$ =0 mm) on, EDL position was manipulated by moving both of its FTs (increments=1mm), 8mm distally until the end distal position ($\Delta posit_{EDL}$ =8mm) was attained.

position. EDL muscle position was changed first by moving its proximal and distal FTs by 5 mm proximally. From this proximal starting position ($\Delta posit_{EDL}$ =0mm) on, EDL position was manipulated by moving both of its FTs in 1mm increments for a total of 8 mm in the distal direction until the end distal position ($\Delta posit_{EDL}$ = 8mm). At each different EDL position, EDL, TA and EHL forces were measured simultaneously.

### 3.1.5 Histological analysis of effects of BTX-A on intra- and epimuscular connective tissue content in combination

In our previous study(Ates and Yucesoy, 2013), histological analyses were performed after employing the BTX-A injection protocol described above. One finding was that BTX-A administration causes partial paralysis of all muscles of the anterior crural compartment following TA injection. We believe this is relevant for the present experiments also. Therefore, it is important to note that intactness of the compartment describes a lack of interference with the EMFT pathways within the compartment, but it does not refer to a lack of BTX-A exposure of the non-injected muscles.

Another finding was that the intramuscular connective tissue content for muscles of the BTX-A group was significantly higher than that for muscles of the control group. Presently, intra- and epimuscular connective tissue content was analyzed in combination such that the region of interest includes the extracellular matrix (ECM) in part and structures interconnecting neighboring muscles such as direct collageneous connections between their epimysia and neurovascular tracts. Changes determined in such intra- and epimuscular connective tissue content due to BTX-A administration were interpreted with reference to the previous findings [67].

We used Gomori Trichrome stain (30-30110; Bio-Optica Milan, Italy) in an additional set of male Wistar rats and divided them into 2 groups: Control (n=4, body mass=355±20g mean± SD), and BTX-A injected (n=4, body mass=343±8g mean± SD). 5 days post-injection (protocol described above), the AC compartment was removed surgically as a whole. This allowed epimuscular connective tissues of the TA, EDL, and EHL to be left intact. Subsequently, the tissues were fixed and processed immediately using an automated tissue processor (TP1020; Leica Microsystems, Wetzlar, Germany) and embedded in paraffin (EG1150H; Leica). 6thick sections were cut using a microtome (RM2255; Leica) for every 20and stained with Gomori Trichrome. The EHL muscle fibers originate from the anterior intermuscular septum and insert on a distal aponeurosis [33] such that the central parts of the EHL belly correspond approximately to the mid section of the AC compartment. Taking this into account,

stained sections from the mid-section of the AC compartment, where all the muscles of the compartment and their epimuscular connections are present were selected and photographed (DM2500; Leica).

### 3.1.6 Data Processing and Statistics

*Muscle mechanics analyses* Passive isometric forces (Fp) were determined 100ms after the second twitch, and total isometric forces (Ft) were determined during the tetanic plateau (the mean force for a 200ms interval, 150ms after evoking tetanic stimulation). Data for Ft in relation to muscle position were fitted with a polynomial function using a least squares criterion:

$$y = b_0 + b_1 x + b_2 x^2 + ... + b_n x^n \tag{3.1}$$

where y represents Ft and x represents $\Delta posit_{EDL}$. $b_0$, $b_1$ ... $b_n$ are coefficients determined in the fitting process. Data for $F_p$ in relation to muscle position were also fitted in the same way. Active forces were estimated by subtracting passive force from the total force for each $\Delta posit_{EDL}$.

Polynomials that best described the experimental data were selected by using one-way analysis of variance (ANOVA) [74]. The lowest order of the polynomials that still added a significant improvement to the description of changes of muscle position and muscle force data were selected. For each muscle studied, muscle forces at different EDL positions were obtained by using these functions. For each $\Delta posit_{EDL}$, forces were averaged, and standard deviations (SD) were calculated to determine muscle force (mean$\pm$SD).

Two-way ANOVA for repeated measures (factors: $\Delta posit_{EDL}$ and animal group) was performed separately for the forces of each muscle. Differences were considered significant at $P<0.05$. If significant main effects were found, Bonferroni post-hoc tests were performed to further locate significant force differences within the factors [74].

Spearman rank correlation coefficients were calculated to test if reductions in EDL total forces due to BTX-A injection are correlated with EDL relative muscle position. Reduction in force is calculated as the difference in mean force between the control and BTX-A animal groups at each EDL relative position. Correlations were considered significant at $P<0.05$.

Histological analyses Intra- and epimuscular connective tissues were analyzed quantitatively to assess whether changes occurred in the collagen content in the AC compartment as a result of BTX-A injection. One-Step Gomori trichrome stain is used to distinguish muscle fibers (stained red-purple) and connective tissue collagen (stained light green). The ratio of collagen content to the cross section of the compartment was determined with a custom-programmed code (MATLAB, R2012a). For both control and BTX groups, the percentage of intra- and epimuscular connective tissue content in the cross-sections was quantified from the images.

For the analyses, 2 separate regions were distinguished on the stained sections in order to establish maximum possible coverage of the connective tissues between the muscles of the compartment with an optimum imaging resolution: the area in which the connective tissue linkages between the EDL, EHL, and TA, including the neurovascular tracts, are present (region I) and the area adjacent to region I, in which the connective tissue linkages between the EDL and TA are present (region II). These regions were determined by taking the neurovascular tracts located at the intersection of the EHL, TA, and EDL as a reference. Initially, photographs with 4X magnification were used to distinguish general structural differences. This was used as a guide for taking photographs with 10X magnification of the described regions. One-way ANOVA was performed to test the effects of BTX administration on regions II and I separately. Differences were considered significant at $P<0.05$.

## 3.2 Results

### 3.2.1 Effects on TA and EHL

Significant main effects of only BTX-A injection on active forces of TA and EHL muscles were found. Respectively, for high and low length conditions, TA active forces decreased by 65.6% and 67.4% (Figure 3.2a, c), and EHL active forces decreased by 41.6% and 50.1% (Figure 3.2b, d).

Significant main effects of BTX-A injection as well as $\Delta posit_{EDL}$ were found only for the EHL passive forces (control group mean values equal 0.01N for both conditions) causing an increase (up to 7-fold).

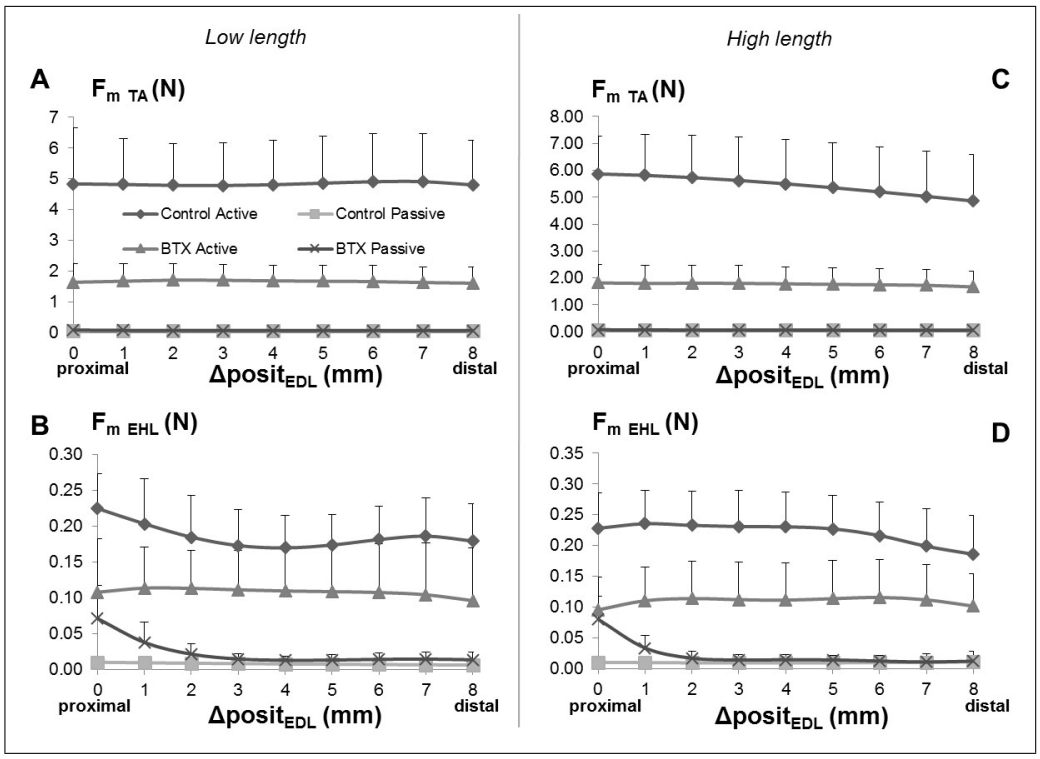



**Figure 3.2** Forces of the TA and EHL muscles as a function of changing EDL relative muscle position. Active and passive isometric muscle forces are shown as mean value ± SD for the control and BTX groups. TA (A) and EHL (B) forces obtained in the low length condition. TA (C) and EHL (D) forces obtained in the high length condition. EDL muscle-tendon complex relative position changes ($\Delta posit_{EDL}$) are expressed as a deviation from the proximal starting position ($\Delta posit_{EDL}$ =0mm) to the distal end position ($\Delta posit_{EDL}$ =8mm).

**3.2.1.1 Proximal forces.** *(I) Low length* ANOVA (factors: $\Delta posit_{EDL}$ and animal group) showed significant main effects on EDL active proximal forces (Figure 3.3a) and a significant interaction. Post hoc testing located significant major effects of BTX-A injection for all $\Delta posit_{EDL}$. A significant perfect negative correlation was found between force reductions as $\Delta posit_{EDL}$ changes from proximal to distal location. The Spearman rank correlation coefficient was -1.0 (P=0.0001).

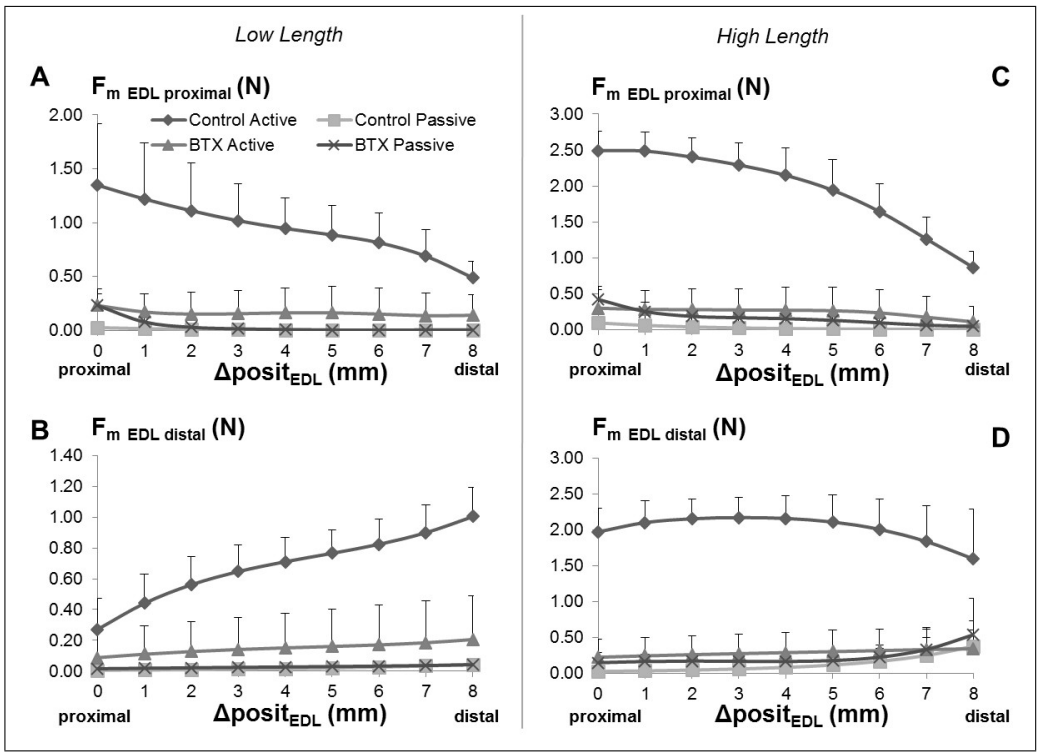



**Figure 3.3** Forces of the EDL muscle as a function of changing EDL relative muscle position. Active as well as passive isometric muscle forces are shown as mean value ± SD for the control and BTX groups. EDL proximal (A) and EDL distal (B) forces obtained in the low length condition. EDL proximal (C) and EDL distal (D) forces obtained in the high length condition. EDL muscle-tendon complex relative position changes ($\Delta posit_{EDL}$) are expressed as a deviation from the proximal starting position ($\Delta posit_{EDL}$ =0mm) to the distal end position ($\Delta posit_{EDL}$ =8mm).

For the control group, EDL force measured at 0mm (1.4±0.6N) decreased significantly with altered $\Delta posit_{EDL}$ (to 0.5±0.2N at 8mm). In contrast, for the BTX group, EDL force measured at 0mm (0.2±0.1N) did not change significantly with altered $\Delta posit_{EDL}$.

ANOVA also showed significant main effects on EDL passive proximal forces, and a significant interaction. Post hoc testing showed significant effects of BTX-A

injection at $\Delta posit_{EDL}$ =0 and 1 mm: Passive force increased about 7-fold due to BTX-A injection.

*(II) High length* ANOVA (factors: $\Delta posit_{EDL}$ and animal group) showed significant main effects on EDL active proximal forces (Figure 3.3c), and a significant interaction. The post hoc test located significant major effects of BTX-A injection for all $\Delta posit_{EDL}$. A significant high negative correlation was found between reductions in EDL active force as $\Delta posit_{EDL}$ changes from proximal to distal location. The Spearman rank correlation coefficient was -0.98 (P=0.0001). For the control group, the EDL force measured at 0mm (2.5±0.3N) decreased significantly with altered $\Delta posit_{EDL}$ (to 0.9±0.2N at 8mm). In contrast, in the BTX group, the EDL force measured at 0mm (0.3±0.3N) did not change significantly with altered $\Delta posit_{EDL}$.

ANOVA also showed significant main effects on EDL passive proximal forces and a significant interaction. The post hoc test showed significant effects of BTX-A injection at $0 \leq \Delta posit_{EDL} \leq$6mm; passive force increased about 6-fold due to BTX-A injection.

**3.2.1.2 Distal forces.** *(I) Low length* ANOVA (factors: $\Delta posit_{EDL}$ and animal group) showed significant main effects on EDL active distal forces (Figure 3.3b) and a significant interaction. The post hoc test located significant major effects of BTX-A injection for all $\Delta posit_{EDL}$, except $\Delta posit_{EDL}$ =0 mm. A significant perfect positive correlation was found between reductions in EDL active force as $\Delta posit_{EDL}$ changes from proximal to distal location. The Spearman rank correlation coefficient was 1.0 (P=0.0001).

For the control group, EDL force increased significantly for 5mm$>\Delta posit_{EDL}>$ 0mm (from 0.3±0.2N to 0.8±0.2N). In contrast, for the BTX group, EDL force at 0mm (0.1±0.2N) did not change significantly with altered $\Delta posit_{EDL}$.

ANOVA also showed significant main effects on EDL passive forces but no signif-

icant interaction. The passive force increase after BTX-A injection was about 1.5-fold on average.

*(II) high length* In contrast to the effects shown for proximal forces, ANOVA (factors: $\Delta posit_{EDL}$ and animal group) showed only a significant effect of BTX-A injection on EDL active forces (Figure 3.3d), but no significant effects of $\Delta posit_{EDL}$ or a significant interaction. The mean force decrease BTX-A caused for $\Delta posit_{EDL}$ was 85.3±3.4%.

ANOVA also showed significant main effects on EDL passive forces, but no significant interaction. Passive force increase after BTX-A injection was about 2-fold on average.

### 3.2.2 Proximo-distal active force differences

*(I) Low length* ANOVA (factors: $\Delta posit_{EDL}$ and animal group) showed significant main effects on the EDL proximo-distal (Fdistal-Fproximal) active force differences (Figure 3.4a) and a significant interaction. The post hoc test located significant major effects of BTX-A injection for $\Delta posit_{EDL}$, including 0-2 and 8mm. For the control group, the force difference values were as high as -1.1±0.6 N at $\Delta posit_{EDL}$ =0mm and 0.5±0.2N at the $\Delta posit_{EDL}$ =8mm. After BTX-A injection, these values decreased substantially (to -0.1±0.2N at $\Delta posit_{EDL}$ =0mm and to 0.1±0.3N at $\Delta posit_{EDL}$ =8mm).

*(II) High length* ANOVA (factors: $\Delta posit_{EDL}$ and animal group) showed significant main effects on the EDL proximo-distal active force differences (Figure 3.4b) and a significant interaction. The post hoc test located significant major effects of BTX-A injection for most $\Delta posit_{EDL}$ including 0, 1, 7, and 8mm. For the control group, the force difference values were as high as -0.5±0.4N at $\Delta posit_{EDL}$ =0mm and 0.7±0.7N at $\Delta posit_{EDL}$ =8mm. After BTX-A injection, these values decreased considerably also for the high length condition (to -0.1±0.4N at $\Delta posit_{EDL}$ =0mm and to 0.2±0.3N at $\Delta posit_{EDL}$ =8mm).

### 3.2.3 Effects on intra- and epimuscular connective tissue content

Figure 3.5 shows sample histological sections of compartmental connective tissue staining. The percentage of intra- and epimuscular connective tissue content values for the BTX group (mean±SD=4.6±2.0% and 8.9 ± 3.6% for regions I and II, respectively) were significantly lower than those for the control group (mean ± SD=6.5 ± 2.0% and 13.0 ± 5.3% for regions I and II, respectively) ($P<0.01$).

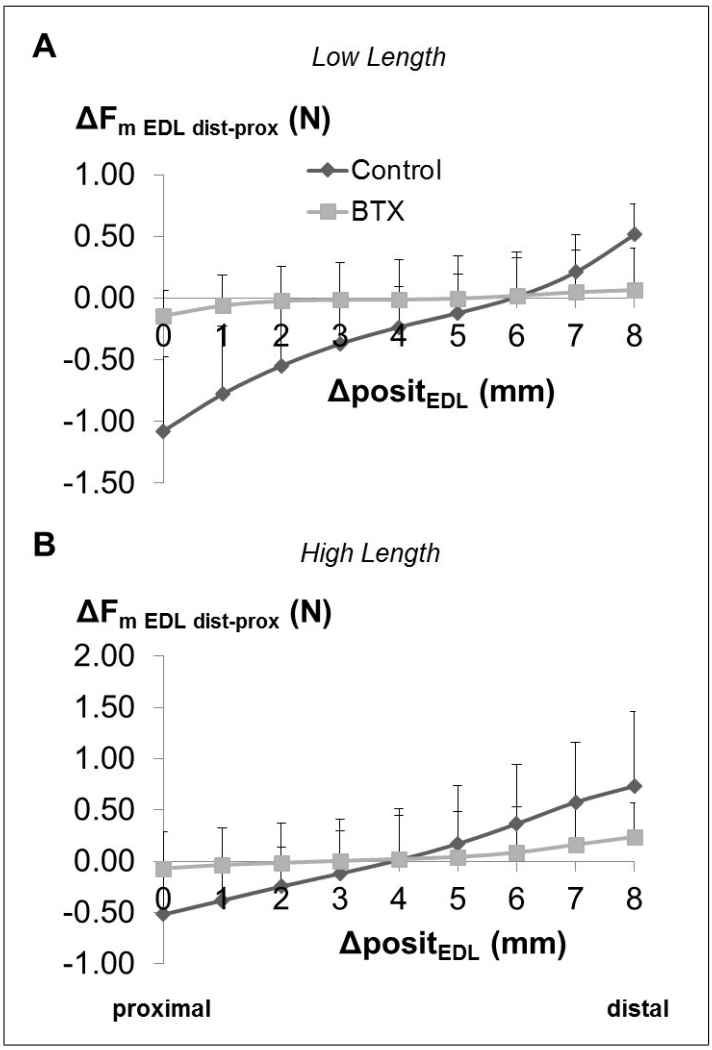



**Figure 3.4** EDL proximo-distal active force differences as a function of changing EDL relative muscle position. The force differences calculated as Fdistal-Fproximal for the control group and the BTX injected group of animals are shown as mean value±SD (A) in the low length condition and (B) in the high length condition. EDL muscle-tendon complex relative position changes ($\Delta posit_{EDL}$) are expressed as a deviation from the proximal starting position ($\Delta posit_{EDL}$ =0mm) to the distal end position ($\Delta posit_{EDL}$ =8mm). Note that a positive force difference indicates that a net epimuscular myofascial load is exerted on the EDL in the proximal direction, and a negative force difference indicates a distally directed net epimuscular myofascial load.

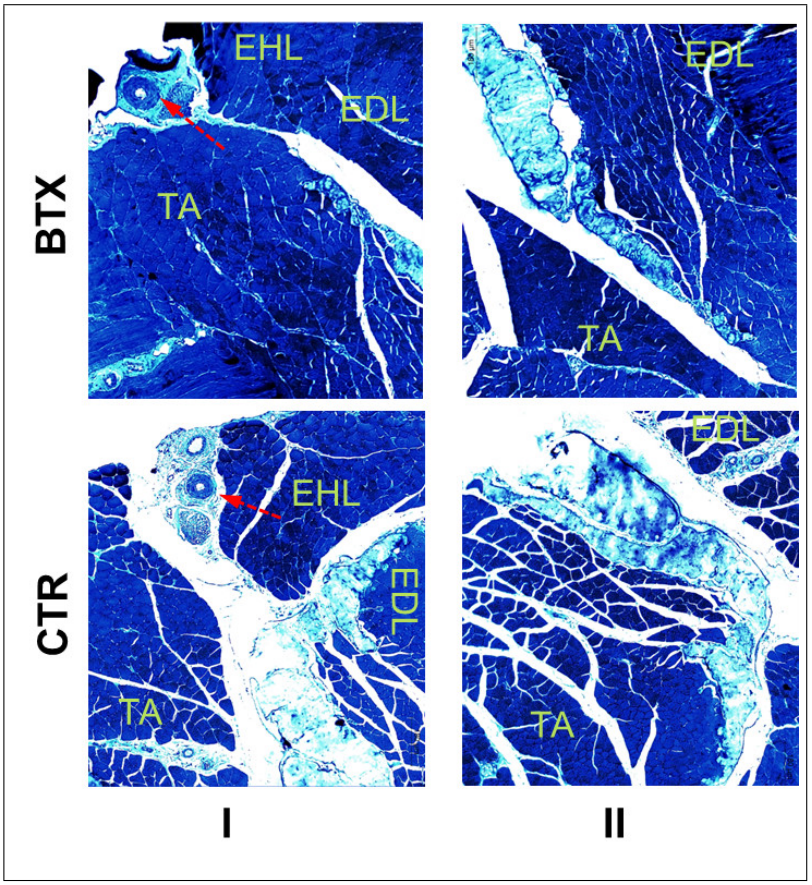



**Figure 3.5** Sample histological sections of AC compartment stained using Gomori trichrome for collagen. The sections show that tissues of the compartment in the TA (left), EHL (top right), and EDL (right) intersect (region I), and at the TA (left) and EDL (right) intersect (region II). Region I involves the neurovascular tracts as well (indicated by dashed arrow). Gomori trichrome stain gives a light (green to blue) color to the connective tissues. The white sections between the muscles involve adipose tissues or are tissue discontinuities due to tissue processing. For a quantitative analysis indicating decreased epimuscular connective tissue content after exposure to BTX-A, see text. CTR: Control Group, BTX: Botox injected.

# 4. SIMULATION OF EFFECTS OF BOTULINUM TOXIN ON MUSCULAR MECHANICS IN DUE TREATMENT COURSE BASED ON ADVERSE EXTRACELLULAR MATRIX ADAPTATIONS CAUSING INCREASED STIFFNESS

Local injections of Botulinum toxin type-A (BTX) are commonly used to reduce spasticity by causing partial muscle paralysis and blocking the hyper-excitable stretch reflexes [44, 45, 7]. However, BTX also affects muscle force substantially [51, 12, 11]. As muscle is the motor for movement, BTX effects on muscular mechanics are functionally extremely important, but the mechanism of these effects and how they change in due treatment course is not well understood. Moreover, no projection is made about the functioning of muscle exposed to BTX, post treatment. Finite element modeling is a powerful tool to assess such mechanisms. Recent modeling of effects of BTX on muscular mechanics indicates that a vast majority of sarcomeres attain higher lengths than identical sarcomeres of the muscle, pre-BTX treatment [75]. Such "longer sarcomere effect" (LSE), is characteristic to partial muscle paralyzation per se, ascribed to muscle fiber-extracellular matrix (ECM) interactions [56]. Remarkably, modeling indicates that LSE can lead to an enhanced potential of active force production of the non-paralyzed muscle parts and a decreased length range of force exertion ($l_{range}$) of muscle exposed. Therefore, BTX effects on muscular mechanics may not be limited to only a force reduction. Recent animal experiments confirm that and show additional to a decreased $l_{range}$, also other so far unknown BTX effects including increased passive muscle force [55, 11, 76]. This is ascribed to an enhanced collagen content of the ECM, several days post-injection [55]. These findings indicate for the longer-term presence of muscle tissue adaptations due to BTX, leading to altered mechanical properties of the ECM. Moreover, although no direct information is available on the ECM properties and structure post-BTX treatment, persistence [77] and even an increase of contracture [78] has been reported in BTX treated patients. This suggests that adaptation of the

ECM remains effective also post-BTX treatment.

Taking these issues into account and using finite element modeling we aimed at simulating the time course of effects of BTX on muscular mechanics based on LSE and ECM adaptations. Specifically, we tested the following hypotheses: (1) enhanced potential of active force production and decreased $l_{range}$ effects elevate with increased ECM stiffness, long-term BTX treatment, and (2) if such adapted ECM properties are persistent, these effects not allied with the treatment aims are also persistent, post-BTX treatment.

## 4.1 Methods

### 4.1.1 Modeled BTX cases

To assess the mechanism of effects of BTX treatment in due treatment course, four cases were modeled: (1) Pre-BTX treatment represents BTX-free muscle. Therefore, the entire muscle is fully activated. (2) Acute-BTX treatment represents effects of BTX immediately after paralyzation settles down. Partial muscle paralysis was modeled by leaving the middle half of the model inactive (paralyzed parts) and fully activating the remaining half (activated parts) (Figure 4.2b). (3) Long-term-BTX treatment models an added representation of ECM adaptations due to BTX. Therefore, constitutive equations of elements modeling the ECM are manipulated for stiffer mechanical properties (see the subsequent section). (4) Post-BTX treatment simulates mechanics of BTX treated muscle after partial muscle paralysis ceases. This is operationalized by maintaining adapted ECM properties, but by fully activating the entire muscle.

### 4.1.2 Description of the model

Using a two-domain approach, a 3D-finite element muscle model (linked fiber-matrix mesh model: LFMM model) was developed [27]. This model consists of two

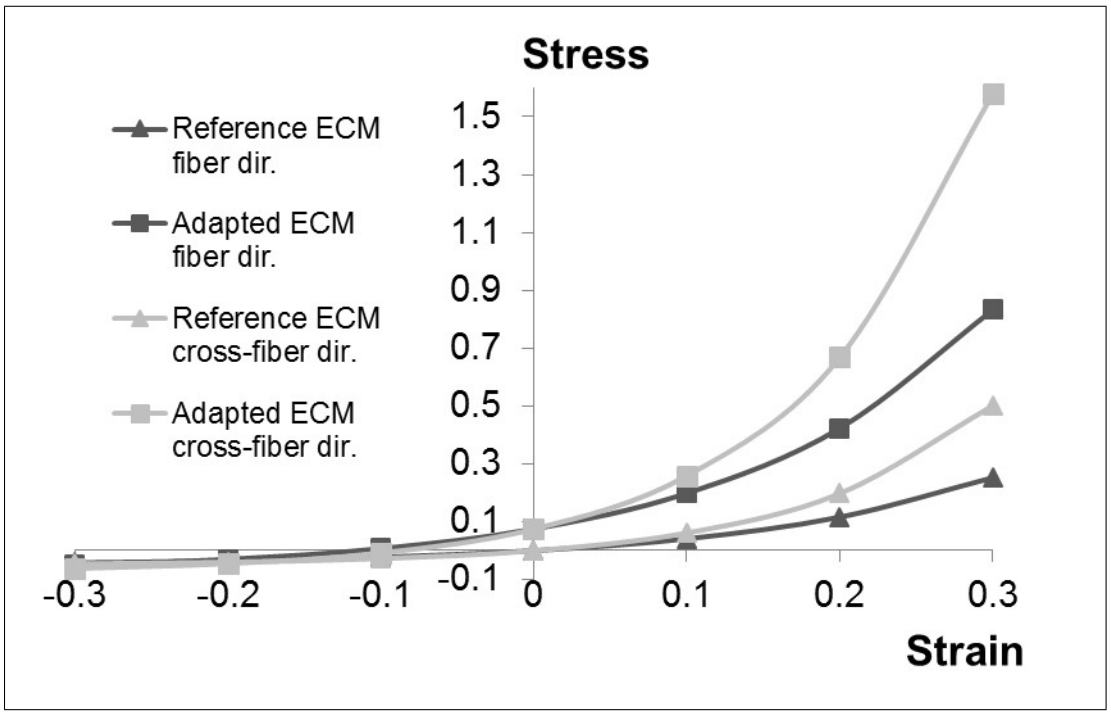



**Figure 4.1** Nonlinear and anisotropic material properties of the extracellular matrix element in the local coordinates. The stress-strain characteristics of the element are shown for the fiber and cross-fiber directions. Material properties of reference ECM represents those of BTX free muscle [79]. Material properties of adapted ECM represents those of BTX-treated muscle. Note that the latter models the principles of muscle tissue adaptations shown to occur experimentally for the rat EDL muscle [55]. An assumption was made that the adapted ECM material properties remain representative of the long-term-BTX and post-BTX treatment cases in an identical way. The stresses are normalized and dimensionless. The reader is referred to a review on LFMM model for full details [11].

meshes, occupying the same space, that are linked elastically. These meshes represent the ECM domain (matrix mesh) and intracellular domain (fiber mesh). Such modeling allows assessment of effects of muscle fiber-ECM interactions.

The two meshes are built using the self-programmed myofiber and ECM elements that were introduced as user defined elements into a finite-element analysis software (ANSYS Academic Teaching Advanced v.12.0 ANSYS. Inc. Canonsburg, PA, USA). The elements have eight nodes and linear interpolation functions. The tissues are considered as a continuum and a large deformation analysis is employed. A 3D local coordinate system representing the fiber, cross-fiber, and thickness directions is used. For the myofiber element, the total stress acting only in the fiber direction equals the sum of the active stress of the contractile elements (representing active force exertion based on overlap of actin and myosin myofilaments) and the stress due to intracellular

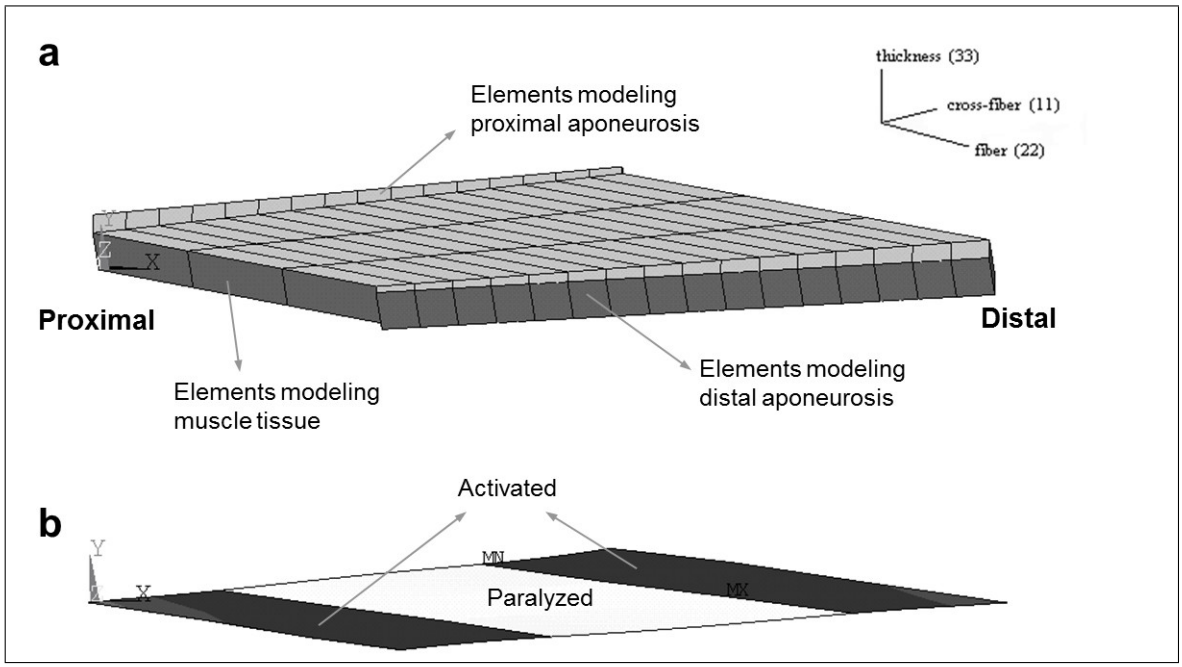



**Figure 4.2** Finite element modeling of EDL muscle and partial paralysis. (a) The model consists of three muscle elements in series and sixteen in parallel. Each combination of three muscle elements arranged in series constructs a whole fascicle. The muscle elements located proximally and distally are connected to elements representing the muscles aponeuroses. A 3D local coordinate system representing the fiber, cross-fiber (normal to the fiber direction), and thickness directions is used for the analysis and presentation of the model results. (b) Typical deformed shape after distal lengthening of the BTX cases for which partial paralyzation was modeled by not activating muscle elements located in the middle half of the muscle: white areas within the muscle belly indicate paralyzed muscle parts whereas, the darker areas indicate the parts that are activated maximally. The choice of middle half paralyzed model is based on Turkoglu et al. [75], which showed distinct effects of the longer sarcomere effect.

passive tension (originating from the intra-sarcomeric cytoskeleton, with a dominant role played by titin). It is assumed that the sarcomeres arranged in-series within muscle fibers have identical material properties.

The ECM element incorporates a two-component strain energy density function one of which accounts for the non-linear and anisotropic material properties and the other considers constancy of muscle volume.

The former component is described as follows:

$$W_1 = W_{ij}(|\epsilon_{ij}|), \tag{4.1}$$

where

$$W_{\epsilon_{ij}} = k.(e^{a_{ij}.z_{ij}} - a_{ij}.\epsilon_{ij}) \; for \; \epsilon_{ij} > 0 \; or, \tag{4.2}$$

$$W_{\epsilon_{ij}} = -W_{ij}(|\epsilon_{ij}|) \; for \; \epsilon_{ij} < 0 \; and \; i \neq j \tag{4.3}$$

$\epsilon_{ij}$ are the Green-Lagrange strains in the local coordinates. The indices $i = 1, ..., 3$ and $j = 1, ..., 3$ represent the local cross-muscle fiber, muscle fiber and thickness directions, respectively. k is initial passive stiffness constant and $a_{ij}$ and are stiffness coefficients.

Recent experimental testing of rat EDL muscle indicates increased amplitudes of muscle passive force (up to several folds) with shift of non-zero passive force exertion to shorter muscle lengths [55]. For the Long-term-BTX and Post-BTX treatment models, constants are manipulated to impose a representative change in the ECM mechanical properties: compared to the reference ECM mechanical properties (e.g., [27], for the adapted ECM, k is tripled, whereas are left unchanged if i=j or reduced (by 40%) if i. The former allows enhanced normal stiffness also at negative strain and the latter avoids a change in shear stiffness since no information is available for such ECM adaptation. The resulting stressstrain curves are shown in Figure 4.1. For full details including description of remainder constitutive relationships, remainder model parameters and activation procedure; see a review by Yucesoy and Huijing [80].

One *muscle element* (a linked system of ECM and myofiber elements) is defined to represent a segment of a bundle of muscle fibers, its connective tissues and the links between them. Both matrix and fiber meshes are rigidly connected to single layers of standard hyperelastic elements (HYPER58) elements forming the muscles proximal and distal aponeuroses. Standard spring elements (COMBIN39) are used to represent the transmembranous attachments i.e., the elastic links between the two meshes. This is a 2-node spring element, set to be uni-axial and having linear high stiffness representing non-pathological connections between the muscle fibers and the ECM (for an analysis

of the effects of stiff or compliant links, see [27]. Initially, these links have zero length.

The extensor digitorum longus (EDL) muscle of the rat was modeled. This muscle is unipennate with a minimal variation of its muscle fiber directions. The geometry of the model (Figure 4.2a) is defined as the contour of a mid-longitudinal slice of the isolated EDL muscle belly. A whole fascicle is constructed by putting three muscle elements in series. Sixteen of those are arranged in parallel, filling the slice space. A combination of nodes along one side of a fascicle is referred to as a *fascicle interface*.

### 4.1.3 Solution procedure

At the initial $l_m$ (28.7 mm), and in the passive state, the serial sarcomeres within muscle fibers were assumed to be in the undeformed state (i.e., strain equals zero, and sarcomere length approximates 2.5 ). Local fiber strain, as a measure of change of length, reflects lengthening (positive strain) or shortening (negative strain) of sarcomeres.

Static analysis was performed, using a force-based convergence criterion (tolerance=0.5%). Muscle origin was fixed whereas, after activation, the position of the insertion was changed to new isometric lengths.

### 4.1.4 Processing of data

l-F curves were studied to quantify passive and active force changes. All forces are normalized for the maximal total force within the data set.

The mean nodal fiber direction strain per fascicle interface is considered to represent sarcomere length changes and hence a metric for LSE. $l_m$, range studied includes lengths between a short ($l_m$ = 25.2 mm) and a long length ($l_m$ = 30.7 mm).

Mean nodal fiber direction strains are assessed at those lengths.

Muscle optimum length, $l_{mo}$ is determined as the difference of passive and total muscle force. Shifts in $l_{mo}$ of Acute-BTX, Long-term BTX and Post-BTX treatment cases are compared to that of Pre-BTX treatment case within the range of muscle lengths studied. Additionally, muscle active slack lengths of each case are determined and their $l_{range}$ is calculated as the difference of that and $l_{mo}$.

## 4.2 Results

### 4.2.1 Longer/shorter sarcomere effect

*Effect of partial muscle paralyzation per se* A characteristic effect is LSE: For all muscle lengths, Acute-BTX treatment mean fiber direction strain curves are localized above those of Pre-BTX treatment (Figure 4.3).

However, modeled BTX induced ECM adaptation causes remarkable changes to LSE:

*(I) Long-term vs. Acute-BTX treatment* The LSE gets more pronounced at shorter (Figure 4.3a) and less pronounced at longer (Figure 4.3b) muscle lengths e.g., mean fiber direction strain values are up to 19.9% higher, Long-term-BTX treatment.

*(II) Post vs. Pre-BTX treatment* At shorter muscle lengths (Figure 4.3a) the LSE remains permanent. Contrastingly, a shorter sarcomere effect (SSE) occurs at longer (Figure 4.3b) muscle lengths: on average, mean fiber direction strain values are 28.7% smaller, Post-BTX treatment.

These findings mean that sarcomeres of BTX treated muscle for both long-term and post-treatment can attain lengths closer to their optimum length of their l-F curves, which favors active force production.

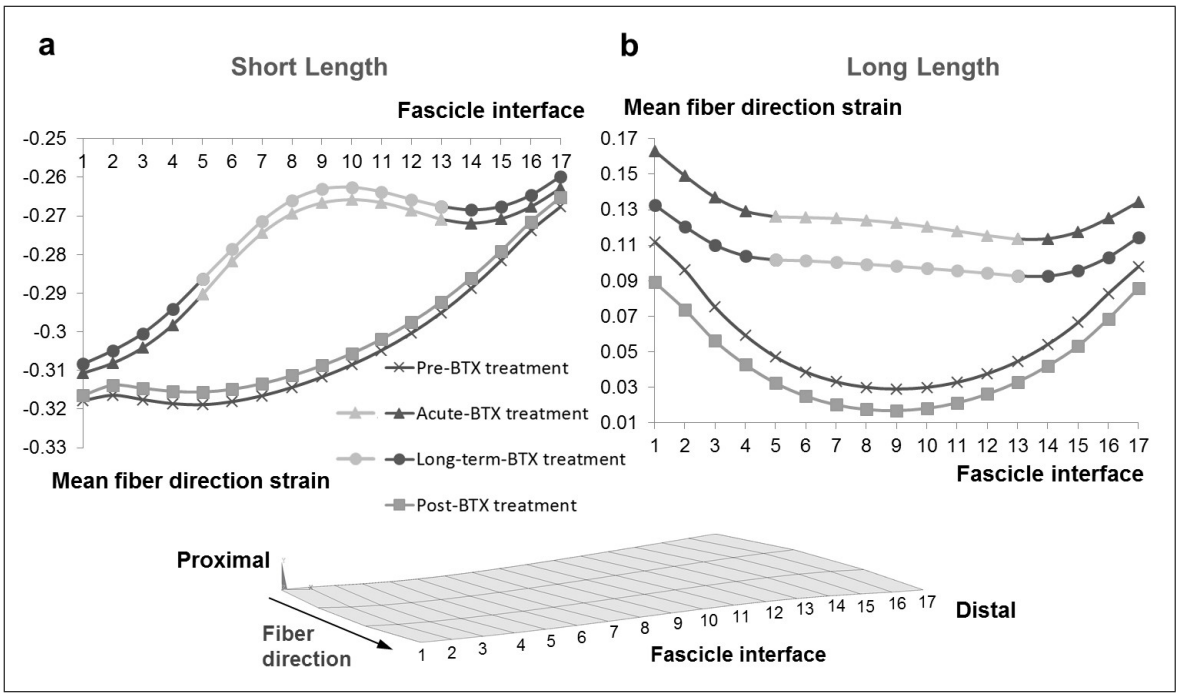



**Figure 4.3** Simulated effects of different phases of BTX treatment on distribution of muscle fiber direction mean strain. In the strain plots activated (dark lines and dark bullets) and paralyzed (lighter lines with lighter bullet filling) muscle parts are distinguished. Muscle lengths considered are (a) Low length ($l_m$ = 25.2 mm) and (b) High length ($l_m$ = 30.7 mm). Mean strain distributions are shown for Pre-BTX treatment, Acute-BTX treatment, Long-term-BTX treatment and Post-BTX treatment cases. For Acute-BTX treatment and Long-term-BTX treatment cases, fascicles 5-13 (middle half of modeled muscle) are paralyzed while fascicles 1-5 13-17 are activated maximally. For the other two cases, all fascicles are activated maximally. Lower panel: A combination of nodes along one side of a fascicle is referred to as a fascicle interface. Each fascicle interface is indicated from by a number from 1 to17. Muscle fiber direction mean strain value for each fascicle interface represents the average value of the strains calculated the four nodes along the interface.

### 4.2.2 Enhanced active force production capacity

*Effect of partial paralyzation per se* A characteristic effect is enhanced active force production (of activated muscle parts): except for a few fascicle interfaces, Acute BTX treatment mean fiber direction stress curves of the activated parts are localized above those of Pre-BTX treatment (Figure 4.4). However, modeled BTX induced ECM adaptation causes remarkable changes to force enhancement:

*(I) Long-term vs. Acute-BTX treatment* Force production capacity of activated sarcomeres gets further enhanced (up to 7.2%) at both shorter (Figure 4.4a) and longer (Figure 4.4b) muscle lengths, long-term BTX treatment.

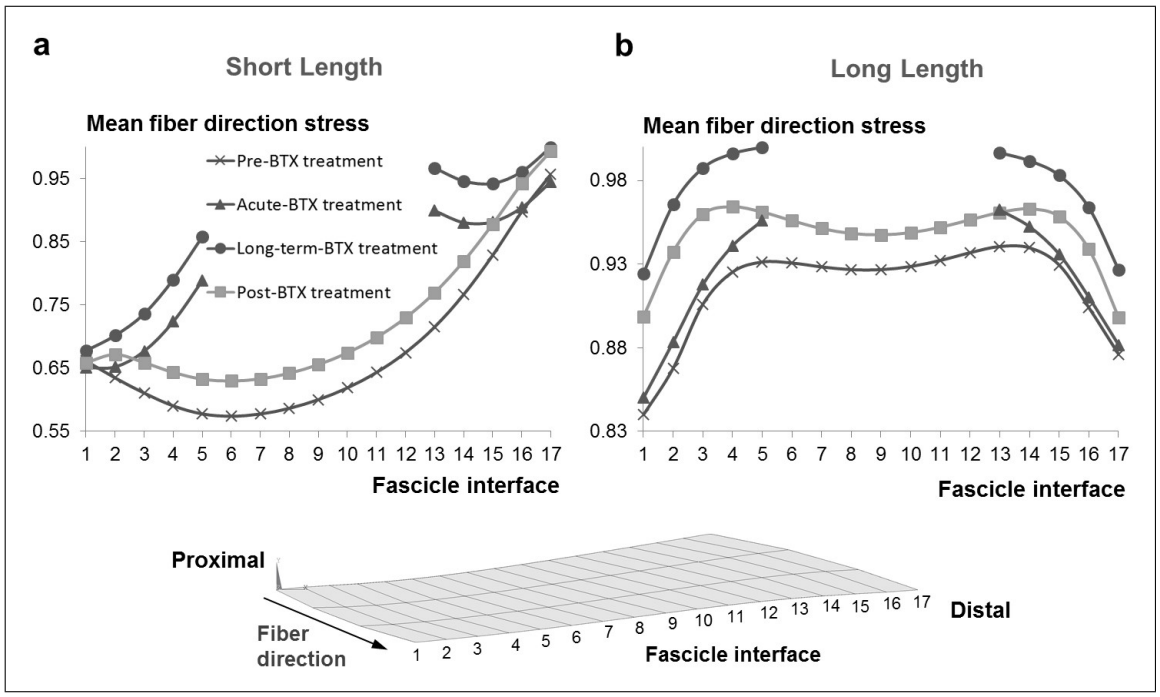



**Figure 4.4** Simulated effects of different phases of BTX treatment on distribution of muscle fiber direction mean stress. Muscle lengths considered are (a) Low length ($l_m$ = 25.2 mm) and (b) High length ($l_m$ = 30.7 mm). As an indicator of active muscle force production, muscle fiber direction mean stress values for each fascicle interface are shown for Pre-BTX treatment, Acute-BTX treatment, Long-term-BTX treatment and Post-BTX treatment cases. For Acute-BTX treatment and Long-term-BTX treatment cases, fascicles 5-13 (middle half of modeled muscle) are paralyzed while fascicles 1-5 13-17 are activated maximally. For the other two cases, all fascicles are activated maximally. Muscle fiber direction mean stress values are normalized for the maximum value, and shown for only activated fascicles. Lower panel: A combination of nodes along one side of a fascicle is referred to as a fascicle interface. Each fascicle interface is indicated from by a number from 1 to 17. Muscle fiber direction mean stress value for each fascicle interface represents the average value of the stresses calculated the four nodes along the interface.

*(II) Post vs. Pre-BTX treatment* Post-treatment, there is no paralyzed muscle part and remarkably, a substantial enhanced force production capacity becomes permanent for the entire muscle.

### 4.2.3 Narrower active $l_{range}$

l-F curves (Figure 4.5) show effects of modeled BTX induced ECM adaptation as changes to muscle passive forces and $l_{mo}$.

*Effect of partial paralyzation per se* A characteristic effect is a shift of $l_{mo}$ to a

shorter muscle length by 5.2% affecting active $l_{range}$ adversely.

*(I) Long-term vs. Acute-BTX treatment* The effect gets more pronounced with an added $l_{mo}$ shift (resulting $l_{mo}$ shift equals of 21.1%).

*(II) Post vs. Pre-BTX treatment* Some of the added $l_{mo}$ shift is persistent (resulting $l_{mo}$ shift equals 18.4%).

Note that compared to Pre-BTX treatment, a narrower $l_{range}$ (20.3%, 27.1% and 3.4% acute, long-term and post BTX treatment) is a consistent finding.

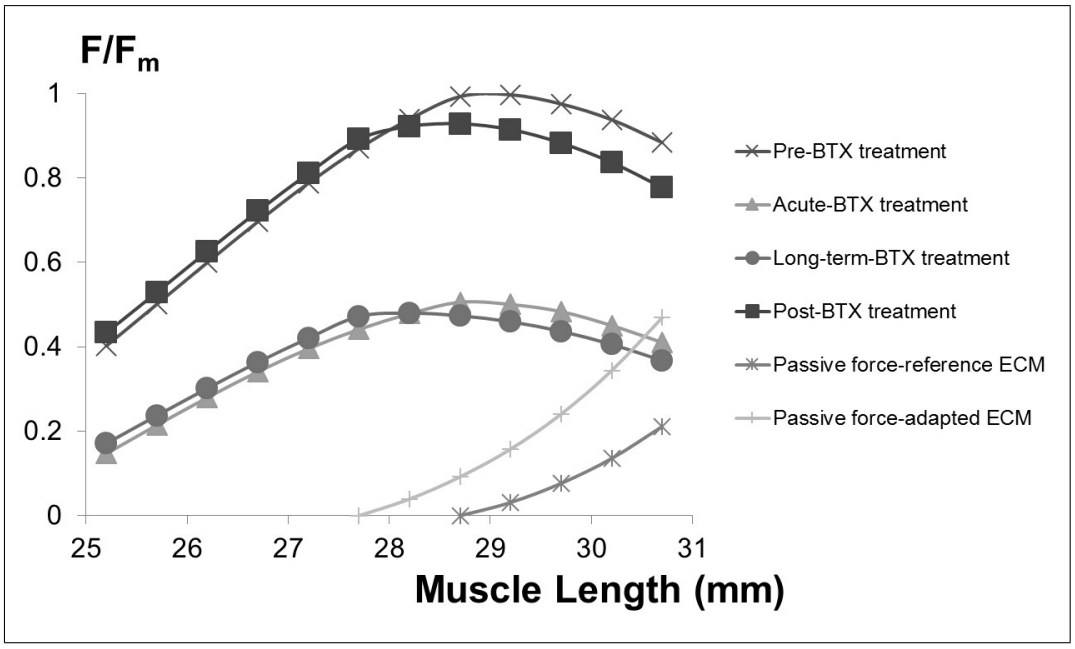



**Figure 4.5** Simulated effects of different phases of BTX treatment on muscle length-force characteristics. The isometric muscle length-force curves for the muscles modeled. Isometric active and passive force curves of Pre-BTX treatment, Acute-BTX treatment, Long-term-BTX treatment and Post-BTX treatment cases are shown as a function of muscle length. All sets of data are normalized for maximal active force of Pre-BTX treatment case.

# 5. DISCUSSION

The results in this thesis reveals the mechanical mechanism of the Botulinum toxin over the entire course of treatment from an individual muscle level to an epimuscular level. The inductive progression of the research is achieved by starting from assessment of effects on individual muscle in chapter 2: length-dependent force reduction effect of BTX treatment is shown to be a result of interactions between activated and paralyzed parts within the muscle. In continuation to reach an epimuscular level, the mechanics of BTX treated muscle in-vivo is studied. In vivo muscle interacts with its environment mechanically, i.e. epimuscular myofascial force transmission, and a new mechanical mechanism would be established after any intervention. Counterintuitively, understanding the effects of the treatment over its time course is shown to lie in the change of the mechanical properties of the individual muscle rather than its interaction with other muscular and non-muscular tissue. The animal experiments in chapter 3 revealed that after BTX injection, mechanical interactions of the muscle with its surrounding muscle ceases to exist and the material stiffness within the muscle increases. Consequently, assessing the time course of the treatment became a determinant of individual muscle properties and mechanics. Therefore chapter 4 focuses on the mechanical changes in the muscle with increased stiffness due to BTX and its consequences if the stiffness change is permanent. In this chapter, specific results, their implications and limitations of the methodologies are discussed in detail.

## 5.1 Mechanisms of modeled effects of BTX in isolated muscle

In Chapter 2, our results show that a mechanism is active that involves length changes of sarcomeres affecting l-F curve, yielding a length-dependent $F_{reduction}$. The key parameter of this mechanism is LSE characterized by MFT via muscle fiber-ECM interactions (e.g., [25]). In BTX-free muscle, MFT has been shown to limit shortening of muscle fibers after tenotomy [25] and aponeurotomy [81, 30]. Such interventions cause numerous muscle fibers to loose their myotendinous connection to the muscular

origin or insertion. However, muscle fiber-ECM interactions prevent sarcomeres from shortening to their active slack length, on activation. Within paralyzed muscle parts of the BTX-cases, muscle fibers cannot shorten due to lack of excitation. Note that by MFT, this effect is also exerted on activated muscle fibers causing LSE. For most $l_m$ studied presently, sarcomeres are at the ascending limb of their individual l-F curve. Due to LSE, active sarcomeres within a BTX-treated muscle can produce more force at identical $l_m$ compared to their counterparts in the BTX-free muscle. This also suggests that the net $F_{reduction}$ originates from paralyzed muscle fibers, but is compromised in variable degrees by active ones. However, as a consequence of LSE, active sarcomeres at the descending limb of their l-F curve exert less active force, whereas passive force originating from intracellular titin increases. Yet, also at longer muscle lengths, even within the same muscle fiber, different sarcomeres will be active on both ascending and descending limbs, [29, 34]. In BTX-free muscles in vivo, magnetic resonance imaging analyses showed the feasibility of simultaneously occurring local lengthening and local shortening [35, 65]. Therefore, for longer lengths, the situation is a complex one. As a general effect, $F_{reduction-comp}$ is shown to be low at shorter lengths, increases to a peak value at intermediate lengths, and decreases again with further increasing $l_m$. This pattern agrees with that of $F_{reduction}$ and therefore $F_{reduction-comp}$ is indicated as a good parameter to explain BTX-induced length dependence of $F_{reduction}$. However, it is not reliable for comparing different BTX-cases because it does not provide a direct comparison between them. For example, although a greater $F_{reduction-comp}$ is shown for case DHP ($26.0<l_m<28.4$mm), $F_{reduction}$ is always greater for case PHP.

*LSE and muscle mechanics.* Model results show more pronounced LSE if the paralyzed part of the muscle is bound by activated muscle parts. This suggests that a more distributed pattern of paralysis may enhance complexity of effects on l-F curve. Such distributed patterns of paralyzed-activated muscle parts are likely if multiple injection sites are used [6, 82]. However, a smaller paralyzed volume may diminish effects, regardless of locations. LSE affects l-F curve by manipulating $F_{reduction}$, which can be a favorable effect. Previous studies reported more pronounced $F_{reduction}$ at shorter $l_m$ [10, 11] or at corresponding joint angles [15]. Yucesoy et al. [11] showed that such differences can be substantial ($F_{reduction}$ equals 55.9% at short and 46.6% at

long $l_m$). In spasticity, muscle hypertonicity [83, 84, 85] is thought to cause the joint to be forcefully kept typically in a flexed position with flexor muscles at short lengths. If this were the case, the desired effect is to obtain a more pronounced $F_{reduction}$ for such lengths. Additionally, spastic muscle weakness itself has been considered as an important source of functional problems (e.g., [53]. In general higher force exertion of activated muscle parts within a BTX-treated muscle can be considered as an asset for controlling the level of $F_{reduction}$ , and hence the produced weakness. However, another consequence of the LSE is that $l_{mo}$ tends to shift to shorter muscle lengths, underlying a potential decrease of the muscle length range of active force exertion [55].

*LSE and stretch-reflex excitability.* BTX has positive effects on spasticity via reduced stretch reflex activity [53], due to a decrease of the reflex muscular tone [44]. However, these effects are ascribable to blockage of gamma-motoneuron terminals in paralyzed muscle parts and not all such terminals are blocked throughout the muscle. Within the activated muscle parts, LSE and potentially longer muscle fibers of intrafusal fibers may cause the stretch-reflex threshold to decrease. Therefore, an increased stretch-reflex excitability of the activated muscle parts may compromise the muscles overall increased stretch-reflex threshold, in agreement with Hesse et al. [86]: most of the chronic hemiparetic patients of that study benefitted from BTX treatment, such that extensor muscles of their lower limb showed a reduction in overall stretch-reflex excitability. However, the EMG patterns of a majority of these patients were classified as type I altered motor control indicating premature clonogenic activity of the soleus muscle, still corresponding to an elevated stretch-reflex excitability.

In conclusion, a key component of mechanisms of how BTX secondarily affects the muscle mechanically is the longer sarcomere effect. Activated muscle parts show an enhanced active force exertion that counteracts the force reduction. Therefore, the size of net force reduction is determined by the proportion of paralyzed vs. activated muscle parts not only due to the presence of the former but also because of the compromising role of the latter. Simultaneously, variation of compromise to force reduction with muscle length is a key determinant of muscle length dependence of force reduction. The longer sarcomere effect leads to a tendency of optimum length to shift to lower muscle

lengths. Myofascial force transmission plays a determining role in this characteristic effect. It should be noted that, to fully understand the possible clinical meaning of the findings, they should be confirmed for humans, in new studies. Finally, presence of parts of muscle being activated and others remaining passive is a common occurrence in daily activities. Therefore, the mechanical mechanisms shown may help understanding of also normal muscle function.

## 5.2 BTX-A causes diminished effects of EMFT and a position-dependent force reduction

Animal experimentation described in chapter 3 show that, due to BTX-A, EMFT within the compartment is diminished. This judgment is based on the following. Unlike the control group, in the BTX group: (i) EDL force measured at the most proximal position did not change significantly with altered $\Delta posit_{EDL}$; (ii) EDL proximo-distal force differences became minimized; and (iii) altered $\Delta posit_{EDL}$ did not cause changes in the forces of TA and EHL muscles. These findings confirm our hypothesis. Ascribed to diminished EMFT, the results show that BTX-A has relative muscle position-dependent force reduction effects.

Proximo-distal force differences represent the resultant of myofascial loads acting on the muscle, which originate from stretching epimuscular connections. Mechanical properties of these connections are complex. Based on previous studies, they have non-linear force-deformation characteristics [87] and prestrain [33] that are inhomogeneously distributed within a muscle compartment [34]. Therefore, epimuscular myofascial loads are expected to be distributed heterogeneously over the muscle belly and may vary as a function of relative muscle position.

MRI analyses in humans in vivo [35, 65] show that changing the relative position of gastrocnemius with respect to the other lower leg muscles causes major local heterogeneous deformations within all muscles. This, similar to other studies [62, 63, 64],

confirms the effectiveness of epimuscular loads on muscle mechanics. Consequently, even for lengths at which the proximo-distal force difference is close to zero, it is plausible that the resultant force is zero, but not local myofascial loads. However, our findings indicate that for muscle affected from BTX-A, the resultant of myofascial loads becomes trivial. Therefore, in this case, rather than a balance of counteracting epimuscular myofascial loads, their absence appears to be responsible for this effect. This can happen in 2 ways: (1) the epimuscular connections do not get stretched with muscle position changes. In fact, as relative muscle position is manipulated exclusively, the tested conditions should impose length changes of epimuscular connections. Therefore, this possibility is weak. However, BTX-A causes partial muscle paralysis [7, 9], and such parts within the muscles of the compartment are expected to be compliant due to a lack of activation. Hence, it is plausible that displacements arising with muscle position changes are taken up in part by the paralyzed muscle parts. This needs to be explored, e.g., by using a finite element model [75, 27]. (2) The epimuscular connections become ineffective. Ates et al. [67] reported an increased proportion of intramuscular connective tissue content of muscles after BTX-A injection. Their data also indicate muscle atrophy. As such atrophy involves decreased muscle fiber diameter and density [88], they concluded that a net increase of the ECM is tenable. Our findings show that cumulative connective tissue content of the compartment (i.e., intra- and epimuscular connective tissues together) decreased due to BTX-A. Considering the increased intramuscular connective tissue content [67], this suggests that BTX-A causes epimuscular connections that act as pathways for EMFT [61, 56, 38] to degrade in quantity. However, because $\Delta posit_{EDL}$ leads to only minor effects on muscle forces, compromised stiffness of these connections is also plausible. This requires further study.

Note that also in the control group, EMFT was not always effective: (1) distal EDL forces in the high length condition were not affected by $\Delta posit_{EDL}$. Compared to earlier BTX-free tests [59, 36], a plausible effect that did not occur is that as $\Delta posit_{EDL}$ changes from proximal to distal muscle positions, EDL distal force increases. Epimuscular myofascial loads can lead to complex sarcomere length distributions. Previous modeling showed that at high muscle length, sarcomeres operating not only in the descending limb, but also in the ascending limb of their length-force curves are present

along the same fascicles [29, 34, 39]. In this study, it appears that such loads manipulated sarcomere lengths that yield significant changes in EDL proximal force, e.g., by shortening them to lengths unfavorable for force exertion but not in the distal force. Nevertheless, the control group data show EDL proximo-distal force differences and a variation of that with $\Delta posit_{EDL}$. Therefore, EMFT was also effective in the high length condition, but a net effect on the distal forces was not shown. (2) $\Delta posit_{EDL}$ had no significant effects on the TA and EHL muscles in the control group. In a previous BTX-free experiment, $\Delta posit_{EDL}$ was shown to cause the force of the TA+EHL complex to change if these muscles were kept at low length [59]. This indicates the presence of EMFT effects. However, the authors also showed that if this complex is brought from a low length to a high length, the effects of $\Delta posit_{EDL}$ on EDL forces become less pronounced. The TA and EHL muscles were kept at the reference position, which corresponds to an intermediate length. This seems to have limited EMFT between the EDL and its synergists in the control group. Therefore, lack of $\Delta posit_{EDL}$ effects on the TA and EHL muscles in the BTX group may be ascribable to the test conditions as well.

## 5.3 Time course of BTX treatment

Cerebral palsy (CP) is one of the most severe disabilities in childhood and is the most common cause of motor deficiency in up to 3/1000 live births [89]. Hypertonia is associated with exaggerated stretch reflexes resulting from disinhibition due to an upper motor neuron (UMN) lesion [40] which in general, is commonly identified using the term spasticity. In the long-term, altered soft tissue morphology and loss of extensibility lead to contracture formation to accompany spasticity causing impaired function [85] ascribed to typical effects of decreased joint range of motion [90] and increased joint stiffness [91]. Therefore, spasticity management is highly important.

BTX injections represent the gold standard for this purpose. Its targeted paralytic effect dampens overactive skeletal muscle reducing muscle spasticity. Overall, the key aims are three fold. First, increasing joint range of motion during active movement

[92] second, achieving more balanced muscle function [93] and third, increasing passive range of motion [94]. Therefore, overall the goal is to improve or restore joint function. One major issue is that this is implicitly considered as an outcome of spasticity management alone. However, muscle is the motor for movement. Therefore, changes in mechanics of BTX treated muscle should be central to the desired joint function. Hence, mechanism of those changes requires major research attention.

$l_{range}$ and active force production capacity of BTX treated muscle are highly relevant parameters characterizing the first two treatment aims. Finite element modeling was used to understand the mechanism of BTX effects on muscular mechanics [75] through these parameters. Remarkably, partial paralyzation per se was shown to cause a narrower $l_{range}$ and enhanced active force production capacity. Central to these effects is the mechanical interaction between muscle fiber and the ECM domains comprising the muscle. These two domains are linked to each other via macromolecular connections along the full length of muscle fibers [17, 57, 58]. Evidence for muscle fiber-ECM interaction was shown experimentally at various levels including single muscle fiber [20], isolated fiber bundles [21] and whole dissected muscle [23]. Such interaction is very important because this means that forces exerted on a sarcomere by the ECM and sarcomeres of neighboring muscle fibers can manipulate its length, hence its contribution to muscular mechanics. Earlier, muscle fiber-ECM interactions were shown to limit shortening of muscle fibers that lose their connections to the muscular origin or insertion after surgical interventions of tenotomy [25] and aponeurotomy [81, 69]. On activation, sarcomeres of such muscle fibers should shorten to their active slack length, if they are not mechanically restrained. The ECM provides this via their mutual linkages. Taking into account this mechanism is highly relevant for understanding mechanics of BTX-treated muscle. Within paralyzed muscle parts, muscle fibers cannot shorten due to lack of excitation. Through muscle fiber-ECM interactions, this effect is also imposed on activated muscle fibers leading to restrained shortening [75]. Resulting LSE causes $l_{mo}$ to shift to lower lengths and active sarcomeres to attain lengths favorable for force production. Therefore, modeling indicates that effects of BTX on muscular mechanics, immediately after paralyzation settles down are not allied with the expected role of the treated muscle on joint function.

On the other hand, muscle ECM stiffness is a parameter certainly relevant for the third treatment aim. Yet, its effect should not be limited to that. Owing to the mechanism described above, ECM stiffness also affects muscles active parameters. Recent experiments showed consistently, increased passive force of BTX treated muscles [55, 11, 76] indicating enhanced ECM stiffness. The present simulations of long-term BTX treatment show that such ECM adaptations are further antagonistic to the expected role of the treated muscle on joint function. This confirms our first hypothesis. In the clinics, the treatment algorithm typically involves several intramuscular BTX injections at 3-6 months periods between injections. This is frequently followed by orthopedic surgery [94]. Therefore, contracture formation cannot be avoided [77]. We dont know if ECM adaptations shown in animal experiments remain effective at least in part also after expiry of BTX induced targeted paralytic effect. If they do, this alone should be considered as a threat to the aim of avoiding a contracture formation and even an elevator of such effect of spasticity [78]. These issues do deserve specific further testing. However, the present simulations of post-BTX treatment conditions suggest based on a persistent ECM adapted condition assumption that BTX treatment may leave behind a muscle with mechanically even worsened contribution to joint function. This confirms our second hypothesis.

## 5.4 Implications and specific limitations of Animal experimentation

The quantity of BTX-A used in the lower limb muscles of children with CP ranges between 3 to 6U/kg [95, 92], and the volume injected ranges between 2.5 to 8ml/kg [95, 96], whereas the quantity and the volumes we injected were approximately 0.32U/kg and 64/kg, respectively. This injection protocol was determined with regard to Shaari Sanders [9]. These authors tested the TA muscle of the rat after a single mid-belly injection of BTX-A using doses ranging from 0.02U to 20.0U. We chose an intermediate dose of 0.1U and used an injection volume in the same order of magnitude as theirs. The substantial muscle force reductions shown indicate that this dose was

quite effective. However, it is much smaller than typical clinical doses. Additionally, dose and dilution volume values per kg used in other species, e.g., 3.5U-0.23ml in the cat [10] and 1 to 10U-0.04ml in the rabbit, [6] indicate considerable variability. Therefore, a general limitation for animal studies is that an explicit relationship with clinical practice in terms of BTX-A dose cannot be made. On the other hand, injection of BTX-A into the TA muscle causes paralysis in other muscles of the anterior crural compartment as well [67, 11]. BTX-A has been shown to spread through muscle fascia [5]. Its effects beyond the injection site have been reported [72, 95, 73] and are considered to be side effects, [97, 98, 99] because they may make controlling of the effects of the treatment difficult. Therefore, the assessment of such effects is important, and despite their limitations, animal models allow for controlled testing.

Stretch sensitive forms of muscle overactivity, including spasticity, spastic dystonia, and spastic cocontraction are associated with exaggerated stretch reflexes resulting from disinhibition due to an upper motor neuron lesion [100] and can lead to abnormalities such as a spastic gait. Muscle hypertonicity [83, 84, 85] commonly occurs in the lower extremities. BTX-A inhibits presynaptic acetylcholine release and causes muscle paralysis [4]. This effect is therapeutic for decreasing muscle overactivity arising from CP and other etiologies such as stroke [101] and multiple sclerosis [102]. Recently, the forces of the activated spastic gracilis muscle of CP patients were measured directly as a function of knee angle [70]. However, neither a narrow operational joint range of force exertion nor a supreme active resistance capacity to stretch at low length was found. Therefore, the muscle force-joint angle data were not representative of the joint movement disorder. The target spastic muscle was stimulated exclusively. This suggests that the movement deficiency is caused by the integrated abnormal functioning of several muscles upon simultaneous stimulation. This has been ascribed to EMFT [70, 66]. In the characteristic flexed joint positions of CP patients, the spastic muscle is at low length and should have a low capacity for active force exertion. Ates et al. [67] support this, because the spastic muscles in flexed knee position were capable of exerting only a portion (maximally 79%, and minimally 22%) of their peak force. However, the antagonistic muscles attain higher lengths favorable for force exertion. Kreulen et al. [103] showed the presence of EMFT in spastic paresis. Huijing [66] proposed that

inter-antagonistic EMFT, which has been shown to occur within an entire healthy limb [65, 56] is responsible for an enhanced resistance capacity of spastic muscle to stretch. Ates et al. [70] argued that the heterogeneity of the lengths of sarcomeres, [29, 34, 39] within muscle fibers may lead to major shape changes in muscle length-force characteristics [33, 29]. In the case of simultaneous activation of muscles in spastic paresis, much enhanced myofascial loads can conceivably cause such heterogeneity. This can change joint angle-muscle force characteristics to become more representative of the abnormal movement.

As shown in a previous work that used histology [9], our findings show via reduced active forces that BTX-A causes muscle paralysis. Chemodenervation has been shown to cause altered sensory input [44, 46]. Cardoso et al. [48] demonstrated with a meta-analysis that treatment of spastic equinus foot with BTX-A in CP patients produced statistically significant gait improvement. Therefore, reduction of spasticity is plausible via reduction of muscle force and sensory effects of BTX-A. However, our results also show that BTX-A eliminates EMFT, at least temporarily. Therefore, a therapeutic effect in addition to reduction of spasticity can be removal of abnormal integrated functioning of several muscles. In order for this implication to be relevant, it is necessary first to establish the role of EMFT in spasticity. New findings contribute to that, as spastic gracilis stimulated simultaneously with vastus medialis tends to represent the movement limitation better [104]. Second, because short-term effects were tested here it is necessary to determine the long-term effects of BTX-A on adaptation of epimuscular myofascial structures and on EMFT. Whether EMFT plays a role after BTX-A effects cease needs to be assessed further.

Obviously, completely isometric testing is an idealization. Yet, for multi-articular muscles, relative position changes may involve limited muscle length changes[71]. For the gastrocnemius muscle Cleland measured the distance from the superior to the inferior attachment when both knee and ankle were completely flexed and extended and showed that the muscle length remains unchanged [71]. Gruner et al. [105] reported that a substantial portion of the stride of rats includes knee extension together with plantar-flexion or knee flexion together with dorsiflexion. Therefore, multi-articular

lower leg muscles are exposed to simultaneously occurring lengthening and shortening at opposite ends. For the part of human gait cycle, which involves knee extension together with plantar flexion, gastrocnemius length is fairly constant [106]. These findings indicate a reasonable representation of our testing for joint motion in vivo. Position changes of a multi-articular muscle can coincide with decreased length of mono-articular synergistic muscles which was shown to cause more pronounced active force reduction effect of BTX-A [67, 15, 10, 11]. For example, in combined knee extension and plantar flexion, as the gastrocnemius attains a proximal position, the soleus becomes shortened. This implies that, after exposure to BTX-A, the contribution of affected plantar flexor muscles to ankle joint moment is compromised much more at such joint positions. Muscle weakness is the primary source of impaired function in the upper motor neuron syndrome in cerebral palsy [107] with spastic paresis [40]. Excessive muscle weakening has been considered to be an adverse effect [101, 97, 96, 108]. Consequently, BTX-A induced muscle weakening is to be controlled [53]. We suggest that for such control, the possibility for increased weakness at certain joint positions should be taken into account.

## 5.5 Muscle model limitations

Our model is incapable of distinguishing intra- and extrafusal effects and dynamic conditions are not modeled. Such model conditions should be considered in future studies for a more comprehensive understanding of the effects. Note that, the clinical conditions may differ from the modeled ones. Firstly, spastic muscle mechanical properties (for detailed discussions of such properties see Yucesoy  Huijing [30] and Huijing [66]) were not modeled presently. Potential limitations of this were addressed previously for modeling of surgery [30, 69]. Spastic muscle tissue was reported to be stiffer than normal (e.g., [109, 110]. Its collagen content may correlate positively with the severity of the disorder (e.g., [111] suggesting a stiffer ECM. An ECM stiffer than modeled may increase resistance to sarcomere shortening due to enhanced MFT and LSE caused by co-existence of activated-paralyzed muscle parts may even become more pronounced. On the other hand, adaptation to a prolonged shortened state is consid-

ered to yield shortened muscle fibers and a reduction in the number of sarcomeres [112]. However, unchanged fascicle lengths have also been reported [113]. In contrast to what can be expected from a muscle with increased sarcomere lengths [114], Ates et al. [67] showed that at shorter lengths, spastic muscle produces no particularly high force, and at long lengths, muscle force is still comparable to the optimal force. Therefore, possible effects of not modeling adapted fascicle lengths are not immediately apparent because its actual occurrence and direction of adaptation is not clear.

Secondly, paralysis of half of the muscle volume is a model idealization. In animal studies, a certain paralyzed muscle volume was shown near the injection location [9]. However, due to its diffusivity [5], BTX is known to produce a dose dependent gradient of denervation determining the muscle volume paralyzed [6]. In clinical practice, multiple injections are common [115]. Therefore, it is not well defined, which part(s) of BTX-treated muscle are paralyzed and our models are not capable of characterizing why and how such patterns of paralysis exist. On the other hand, a process involving inactivation of synaptosomal-associated protein [116] determines to what extent BTX induces paralysis of fibers. However, muscle fibers are paralyzed entirely by complete inhibition of evoked neurotransmitter release [117, 118]. Therefore, our choice to model fully functional in combination with fully paralyzed muscle fibers is tenable.

Thirdly, representativeness of the model geometry should be discussed (see appendix for full details). Rat EDL is a unipennate muscle with a pennation angle= $9.0\pm1.1^o$ [119], measured as the angle between muscle fibers and the distal muscle tendon. In human, its pennation angle is comparable ($10.8\pm2.8^o$), and fiber length/muscle length ratio ($l_f/l_m$)=$0.24\pm0.04$ [120]. Several of lower extremity muscles subject to BTX-treatment [47] have a smaller (e.g., pennation angle of vastus intermedius= $4.5\pm4.5^o$; $l_f/l_m$ of extensor hallucis longus=$0.31\pm0.06$) or greater (e.g., pennation angle of soleus= $28.2\pm10.1^o$; $l_f/l_m$ of gracilis=$0.79\pm0.08$) pennation angle and $l_f/l_m$ [120]. Therefore, geometric differences do exist among BTX-treated muscles and the present model is not representative of many muscles directly. However, in principle LSE as a result of muscle fiber-ECM interactions is expected to occur in all muscles. Yet, muscle pennation angle may manipulate the effect. In muscles with a small pennation

angle, because a higher fraction of $l_m$ change is imposed on its muscle fibers, global muscle lengthening may cause more muscle fiber stretch. This can enhance the effect. Within more pennate muscles, the opposite is likely. Among similarly pennate muscles, activation may cause muscle fibers to shorten more for smaller $l_f/l_m$ than bigger, particularly at the mid-muscle belly location because active fiber forces are likely to curve a longer aponeurosis more. However, BTX-induced partial-paralysis may limit this and increase the LSE. Not all muscles are unipennate. Within multipennate arrays, the reduced shortening of muscle fibers compensate for the loss of fiber force due to angulation [121] suggesting that LSE will be more pronounced.

It should also be acknowledged that (i) Modeled muscle mechanical properties represent those of healthy muscle, whereas spastic muscle tissue was reported to be stiffer than normal (e.g., [109, 110]. However, we do address here effects of an enhanced ECM stiffness on muscular mechanics representative of the period of spasticity management. Therefore, principles of muscle tissue stiffening are considered. Our experimental findings suggest that BTX may even contribute to that. On the other hand, BTX induced enhanced ECM stiffness is a newly shown effect and it is not known if collagen content increase is more pronounced in certain directions. For healthy rat muscle Jarvinen et al. [122] indicated long axis of the muscle fibers as the main collagen fiber orientation of the endomysium. They reported collagen also running perpendicularly to the long axis interconnecting adjacent muscle fibers, and collagen fibers attached to the intramuscular nerves and arteries. The later two networks may provide also shear resistance of the endomysium. Presently for the adapted ECM properties employed in long-term and post-treatment models we imposed a uniform increase of stiffness in the muscle fiber, cross-muscle fiber and thickness directions to characterize experimentally measured passive force enhancement. Because no report of altered shear stiffness of the ECM is available for BTX-treated muscle, we imposed no shear stiffness change. Note that on immobilization, Jarvinen et al. [122] showed increased collagen content and indistinguishable patterns of the various networks of fibers implying an inhomogeneous orientation of added collagen fibers. Despite being probably a quite different situation compared to BTX induced partial paralysis, this suggests that changes to shear stiffness are not unlikely. These issues require further specific attention. (ii) Entire muscle

fibers get paralyzed by inhibition of neurotransmitter release due to BTX injection [117, 118]. Therefore, modeling completely paralyzed or activated parts within the muscle is tenable. Yet, the paralyzation pattern considered is an idealization because a more complex pattern is plausible owing to multiple injection protocols used in the clinical practice [115]. However, modeling indicates that the more complex the pattern gets, the more pronounced are muscle fiber-ECM interactions and their effects on muscular mechanics [75]. Therefore, the present findings may be considered to represent the general principles of effects of partial paralyzation occurring during the period of spasticity management.

Based on these points discussed above and other potential issues not addressed here, model findings are not to be considered as representative of the treated muscle directly. However, they do raise important points worth elaborating on in future studies. In summary, LSE and its reflection on muscular mechanics are plausible automatic effects of partial paralyzation. Therefore, some adverse effects of BTX on joint function may be inevitable and these can compromise the therapeutic effect of reduced spasticity. It is important to optimize those though. However, with ECM adaptations shown in animal experiments incorporated, the present modeling indicates that this wont be a constant effect in the longer term. Instead, adverse effects on joint function may become more pronounced. This may further compromise benefits of reduced spasticity during the period of spasticity management. Moreover, present simulation of post-treatment condition suggests that when spasticity management is terminated, the treated muscle may become a less suitable motor for already compromised movement of CP patients. A key issue for the long-term- and post-BTX treatment effects is ECM adaptations. This may not only affect muscular mechanics as shown in the present findings, but may even contribute to contracture formation. Therefore, we suggest that this issue is one that future research should focus on.

## 5.6 Future Directions

One of the main results of the experimental study in chapter 3 was the diminished epimuscular myofascial force transmission. The importance of this result is twofold: (1) The intramuscular effects of BTX becomes sole definer of the effects of BTX of that individual muscle if no interaction occurs between muscles. (2) Ates et al. [67] showed that when activated alone spastic Human Gracilis muscle show no abnormal muscular mechanics suggesting interactions between muscles are crucial in abnormal function seen at the joints. The latter reason especially necessitates an explanation to how and under which conditions such an effect arises and to study this loss of interactions, modeling of the entire compartment would be necessary. In the next section a compartment model is described to be used for such purposes.

## 5.7 Model Of Anterior Crural Compartment (ACC) Muscles With Epimuscular Connections

A model of the ACC muscles at their intersection plane (Figure 5.1a) was created to represent the principles of epimuscular myofascial force transmission within the compartment. Geometric measurements of the muscles were used to form a longitudinal slice (Figure 5.1b) of each of the rat ACC muscles: Extensor Digitorum Longus (EDL), Tibialis Anterior (TA) and Extensor Hallucis Longus (EHL).

The muscles are modeled as unipennate in accordance to individual pennation angles and minimal variation of the fiber direction within the muscle bellies. Note that high fiber direction variation at the origin of TA can not be modeled. However this area is limited to less than 1% of the TA muscle length and therefore can be ignored. Muscle volumes were adjusted with experimental data. Three muscle elements in series and sixteen for EDL, two for EHL and eight for TA in parallel fill the model volumes. Therefore any collection of three muscle elements arranged in series represents a muscle fascicle. All aponeurosis elements have identical mechanical properties but

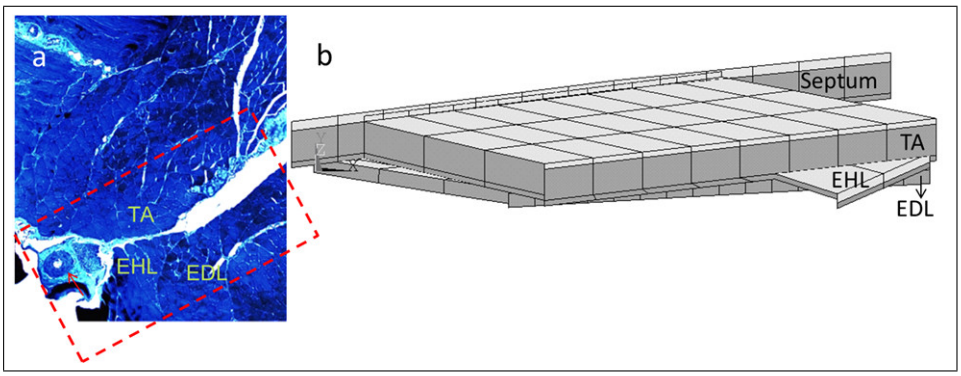



**Figure 5.1** Compartment model representation (a) Histological view of a transverse section of the compartment muscles. The compartment is removed as a whole to keep the muscles, their relative positions and their connections intact. The region modeled and the neurovascular tract are indicated with a red rectangle and arrow. (b) The compartment model geometry.

using a variable thickness in the fiber-cross fiber plane, the increasing cross-sectional area of the aponeurosis toward the tendon [123] is accounted for. Anterior intermuscular septum separating the ACC and Peroneal compartment [31] is modeled as a uniform slab composed of elements with identical mechanical properties for a proper origin of EHL muscle that is also connected to the septum along its length. Direct intermuscular connections at the muscle interfaces due to continuous nature of muscle epimysia are also realized using COMBIN39 element connected at the nodes.

**Table 5.1**
Anterior Crural Compartment Muscles' Dimensions

| | EDL | TA | EHL |
|---|---|---|---|
| **Muscle Length** | 28.7 mm | 25.38 mm | 14.7 mm |
| **Proximal tendon length** | 17.0 mm | - | - |
| **Distal tendon Length** | 19.7 mm | 8.70 mm | 6.8 mm |
| **Muscle width** | - | 3.88 mm (rounded up to 4) | 1.5 mm |
| **Muscle mass** | 0.161 g | 0.588 g | 0.016 g |

Neurovascular tract is the most important link between synergistic muscles mechanically. It is a continuous collagen network, which reinforces the nerves innervating muscle fibers and the blood vessels entering the muscle. The tract is modeled with a main body of spring elements and branches out to represent the extramuscular connective tissue sheets to the muscles. Due to the collagen-reinforced structure, the proximal portions of the these sheets were shown to be much stiffer than the remainder of the

sheet [34]. This is taken into account by stiffer extramuscular links at the proximal nodes. Medially, the tract is connected to the inter-muscular septum and interosseal membrane. To account for such links the tract is also connected to the ground elastically. The spring element COMBIN39 with linear stiffness characteristics was used with different stiffness for the main body, extramuscular links and the septum connections. A suitable stiffness determined previously between the experimental and modeled muscle forces, was used [34].

### 5.7.1 TA Muscle Anatomy And Its Model

Tibialis Anterior (TA) muscle is located laterally in the anterior crural compartment of the rat. It covers the other two compartment muscles i.e., the EDL and EHL and it is 3.6 times and 37 times larger in size compared to EDL and EHL, respectively. The muscle fibers of the TA originate from the proximal head of the tibia and the interosseus membrane (Figure 5.2). In human, the TA is a symmetrically bipennate muscle with a consistent architecture between its unipennate parts [124] except for the most proximal side (app. 7% of muscle length). At the most proximal part, the muscle fibers are attached to the bone at a high fiber direction variation. Distal to this region, the muscle fibers are relatively parallel to the plane on insertion [125]. The TA is a bipennate muscle and hence, the aponeurosis forms inside the muscle. The muscle fibers insert at depths of the muscle in this intramuscular part of the distal TA tendon [125]. Pinned down by the retinaculae at the ankle joint, the distal tendon is attached to the metatarsal bones of the foot.

Several passive structure elements connect the TA to its surroundings. The nerves and blood vessels embedded in sheets of connective tissue (neurovascular tracts) reach the TA and the other muscles of the compartment. Coming from the peroneal compartment and entering through a fenestration in the anterior intermuscular septum into the anterior compartment, the neurovascular tract lies along the interface of the compartment muscles and branches out to the muscles. These connective tissue sheets are continuous with the intramuscular connective tissues and are much denser along

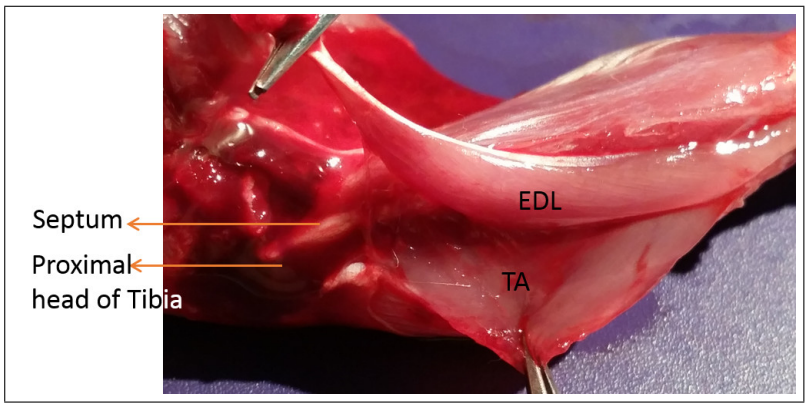



**Figure 5.2** Lateral view of ACC compartment. TA is pulled out to reveal EDL muscle underneath. Origin of TA is dissected from the tibia and septum. EDL is reverted to reveal the proximal aponeurosis.

approximately the proximal 2/5 of the muscle length. Additionally, the frontal part of the epimysium of the TA is thought to be connected with the epimysium of the biceps femoris muscle [31] along with the crural fascia that covers the surface of the TA [60]. Although considered as weak, direct collagenous connections between the TA and other compartment muscles are also present [31].

In our model, the portion of the TA muscle located at the interface with the rest of the compartments muscles is modeled. Figure 5.3 shows a 3D model of EDL, EHL muscles and the septum and a cross-section of the compartment model and the locations of the slices selected to model the three muscles. As such, the TA model represents one of the two parts of the bipennate rat TA. Consequently, it is modeled as a unipennate muscle. In the part of the TA modeled, the muscle fibers have the following origins: Proximal connections to the ground and the septum are present from the muscle body directly without aponeurosis. EDL muscle has its proximal tendon fixed to the ground In order to represent the modeled muscle volume and to operationalize these model choices, two longitudinal muscle slices are developed with proximally the muscle fibers fixed to the mechanical ground (representative of tibial origins) and to the septum and distally inserting to an aponeurosis.

A two-layered TA model is utilized for proper connections to the septum shared with EHL muscle: a layer for the origin of the EHL muscle and a second layer according

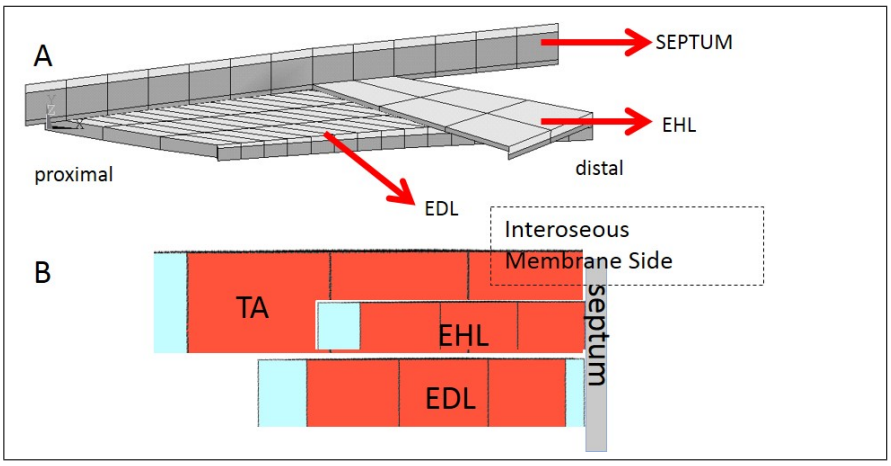



**Figure 5.3** Model representation of EDL and EHL (A) 3D model of EDL, EHL muscles and the septum and (B) a cross-section of the compartment model and the locations of the slices selected to model the three muscles.

to TA volume are developed. Three muscle elements in series and eight in parallel fill each layer. Therefore any collection of three muscle elements arranged in series represents a big muscle fascicle.

Epimuscular connections to the TA muscle consist of (i) the neurovascular tract and (ii) direct collagenous connections to the other compartment muscles. In order to model the muscles epimuscular connections, the matrix mesh was linked at the most proximal 4/9 set of nodes to the neurovascular tract and at the remaining nodes to the other muscles (Figure 5.4) the using spring elements, COMBIN39. The spring elements were set to be uniaxial and have linear length-force characteristics. A stiffness determined previously between the experimental and modeled muscle forces, was used [34].

## 5.8 Conclusion

In this thesis, the changes in the mechanical mechanism of the muscle due to Botulinum toxin treatment have been studied using computational and experimental methods. The computational method, namely finite element model of the muscle, provided valuable mechanical parameters while experimental study on the Wistar rats

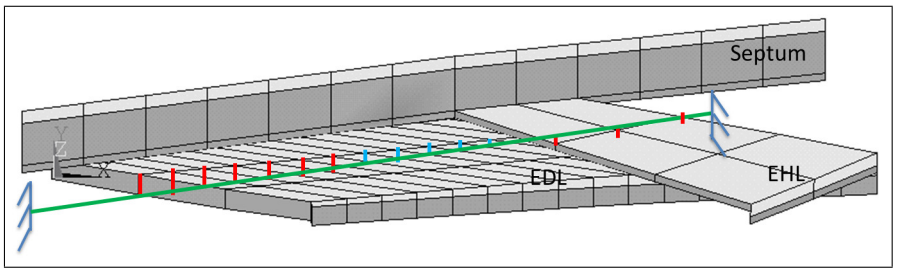



**Figure 5.4** The components of the neurovascular tract and its location. (The TA is removed for visualization). Stiffer connections containing neurovascular (shown with red) and remaining compliant connection (shown with blue) connected to a base tract (shown with green) are shown. As these sheets are continuous with the intramuscular connective tissue of the compartment muscles and non-muscular tissues, the tract is fixed to the ground at both ends.

provided essential inputs that guided the study.

The isolated muscle model of the partial paralysis described in chapter 2 revealed the mechanism causing an increased potential of force production and also explained length dependency of the BTX induced force reduction. Such a system induces a shift of active slack length and therefore decreases the length range of force exertion. Managing the force reduction at different muscle length has functional importance: (i) The hypertonic spastic muscle is thought to limit the flexor muscles to short lengths by keeping the joint at a flexed position [83, 84, 85]. For such a muscle, more pronounced force reduction at short lengths is more desirable. (ii) It is also discussed that muscle weakness itself is a problem in spasticity (e.g., [53]). The increased force production potential would counteract the BTXinduced weakness as a function of length.

The interactions between the fiber and the extracellular matrix, i.e. intramuscular myofascial force transmission, are a key concept in understanding the source of these effects. Moreover, it is also shown that such interactions is not limited to fiber and ECM [56, 29, 69]. The mechanical system within the compartment can be expected to get affected from such changes in the muscle. And the fact that force reduction is seen within the entire compartment [11] due to toxin diffusion [5] increases the likelihood of such an alterations in the intermuscular interactions. However, experimental results in chapter 3 showed an entirely different scenario. Accordingly, the epimuscular myofascial force transmission diminished due to BTX. Additionally, the intramuscular

collagen content and hence the ECM stiffness is shown to increase. Such results proved that in case of BTX application, the effects of the toxin on the individual muscles are central to its mechanical effects.

With such knowledge, our modeling scenario in chapter 4 focused on the time course of the toxin. By manipulating the ECM stiffness of the muscle element of the model, long-term and post-treatment effects of such a property change is studied. It has been shown that in case of a permanent change in stiffness, decreased length range and higher force production due to longer sarcomeres at low lengths may persist: The decreased joint range [90] and increased joint stiffness [91] is ascribed to contracture formation due to tissue property changes. Therefore long term changes in the morphology and shown accompanying adverse mechanical effects are important in management of spasticity.

# APPENDIX A. Description of the "Linked Fiber-Matrix Mesh model"

Using the linked fiber-matrix mesh model (LFMM model [126]) created in accordance with experimental data on muscle properties, skeletal muscle is considered explicitly as two separate domains: (1) the intracellular domain and (2) extracellular matrix domain. The transsarcolemmal attachments are considered as elastic links between the two domains.

Two self-programmed elements were developed and were introduced as user-defined elements into the finite element program ANSYS 9.0: (1) extracellular matrix element represents the collagen reinforced extracellular matrix, which includes the basal lamina and connective tissue components such as endomysium, perimysium and epimysium. (2) myofiber element models the muscle fibers. Within the biological context, each combined muscle element represents a segment of a bundle of muscle fibers with identical material properties, its connective tissues and the links between them. This is realized as a linked system of extracellular matrix and myofiber elements (for a schematic 2D-representation of an arrangement of these muscle elements see [126]). A whole fascicle is constructed by putting three muscle elements in series.

In the LFMM model, the extracellular matrix domain is represented by a mesh of extracellular matrix elements (matrix mesh). In the same space, a separate mesh of myofiber elements is built to represent the intracellular domain (fiber mesh). The two meshes are rigidly connected to single layers of elements modeling proximal and distal aponeuroses: a node representing myotendinous connection sites is the common node of all three (extracellular matrix, myofiber and aponeurosis) elements. In contrast, at the intermediate nodes, fiber and matrix meshes are linked elastically to represent the transmembranous attachments of the cytoskeleton and extracellular matrix. For these links (the model includes a total of 28 of them: 14 in each of the upper and lower model surfaces) the standard element, COMBIN39 is used from the element library of

ANSYS 9.0. This is a 2-node spring element, which is set to be uni-axial and have linear high stiffness characteristics representing non-pathological connections between the muscle fibers and the extracellular matrix (for an analysis of the effects of stiff or compliant links see [126]). Note that at the initial muscle length (28.7 mm) and in passive condition, these links have a length equaling zero.

Extracellular matrix and myofiber elements have eight nodes, linear interpolation functions and a large deformation analysis formulation are applied. A 3D local coordinate system representing the fiber, cross-fiber (normal to the fiber direction), and thickness directions is used. The stress formulation $\underline{S}$ based on Second Piola-Kirchoff definition constitutes the derivative of the strain energy density function, $W$; with respect to the Green-Lagrange strain tensor, $\underline{L}^G$.

$$\underline{S} = \frac{dW}{d\underline{L}^G} \tag{A.1}$$

### A.0.1 Extracellular Matrix Element

The strain energy density function mechanically characterizing the extracellular matrix includes two parts:

$$W = W_1 + W_2 \tag{A.2}$$

The first part represents the non-linear and anisotropic material properties [79]:

$$W_1 = k.(e^{a_{ij}.z_{ij}} - a_{ij}.\epsilon_{ij}) \; for \; \epsilon_{ij} > 0 \; or, \tag{A.3}$$

$$W_1 = -W_{ij}(|\epsilon_{ij}|) \; for \; \epsilon_{ij} < 0 \; and \; i \neq j \tag{A.4}$$

where $\epsilon_{ij}$ are the Green-Lagrange strains in the local coordinates. The indices $i = 1, ..., 3$ and $j = 1, ..., 3$ represent the local cross-fiber, fiber and thickness directions, respectively. $a_{ij}$ and $k$ are constants (Table 2.1). The resulting stress-strain curves are shown in Figure A.1.

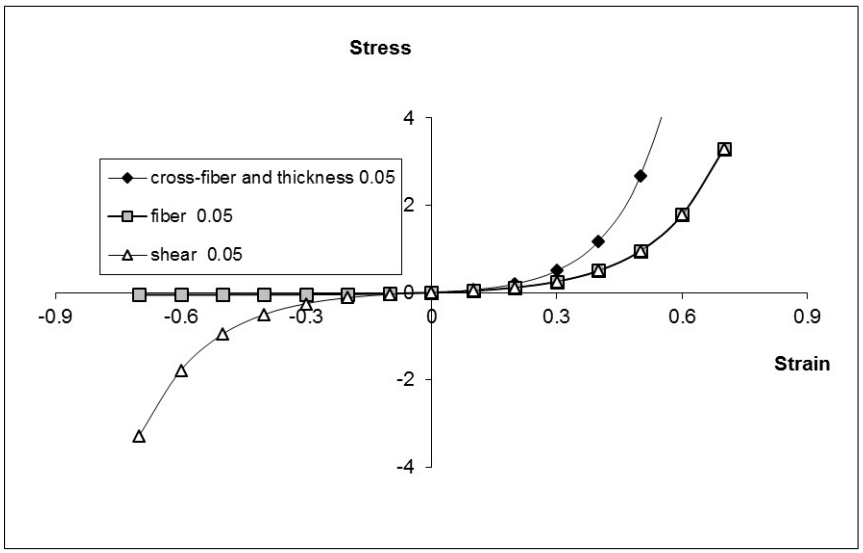



**Figure A.1** Passive non-linear and anisotropic material properties of the extracellular matrix element in the local coordinates

The second part includes a penalty function to account for the constancy of muscle volume

$$W_2 = S_s.(I_3 - 1)^2 + S_f.(I_{avg}^3 - 1) \tag{A.5}$$

where $I_3$ is the third invariant (determinant) of the Right Cauchy-Green strain tensor and is a measure for the local volume for each Gaussian point. To conserve the local volumes (i.e. $I_3$ equals unity), the element is considered as incompressible solid. In contrast, if the weighted mean of all $I_3$s per element ($I_{avg}^3$) is kept as unity, the element is considered to be a fluid. Using the penalty parameters ls (for the solid volume) and lf (for the fluid volume) (Table 1), the emphasis given for each part can be manipulated.

### A.0.2 Myofiber Element

Maximally activated muscle is studied and within the muscle fibers, sarcomeres are assumed to have identical material properties. The force-velocity characteristics are not considered due to the isometric nature of the present work. The total stress for the intracellular domain ($\sigma_{22_f}$) is a Cauchy stress acting only in the local fiber direction and is the sum of the active stress of the contractile elements ($\sigma_{22_{contr}}$) and

the stress due to intracellular passive tension ($\sigma_{22_{icp}}$). To define the active length-force characteristics, an exponential function (Figure A.2) was fit to the experimental data of small rat GM fiber bundles [127]. This function is scaled such that at optimum length, the fiber direction strain ($\epsilon_{22}$) is zero and the maximal stress value is unity,

$$\sigma_{22_{contr}}(\epsilon_{22}) = b_3 e^{b_2 \epsilon_{22}^3} \; for \; \epsilon_{ij} > 0 \; or, \tag{A.6}$$

$$\sigma_{22_{contr}}(\epsilon_{22}) = b_3 e^{b_1 \epsilon_{22}^4} \; for \; \epsilon_{ij} < 0 \tag{A.7}$$

where $b_1$, $b_2$ and $b_3$ are constants

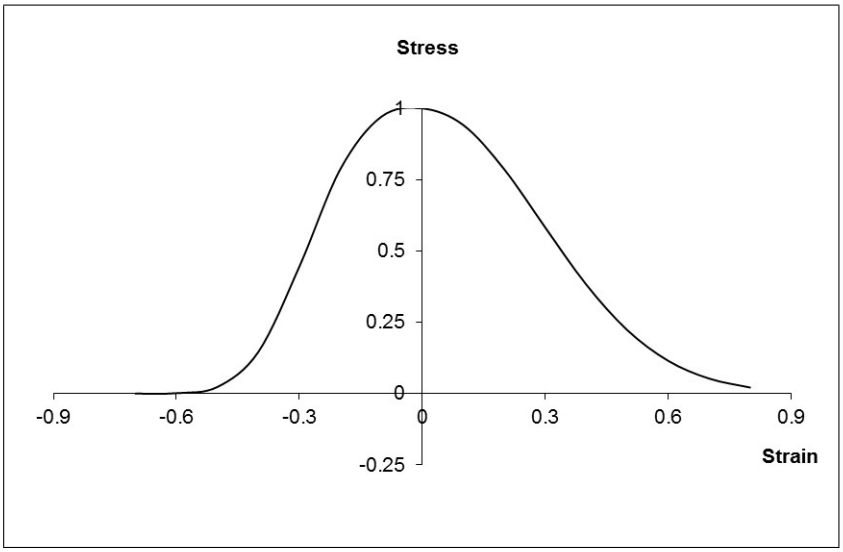



**Figure A.2** Active stress strain properties of the myofiber element representing the contractile apparatus, which is only valid for the local fiber direction

The source of intracellular passive tension is the intrasarcomeric cytoskeleton [128], which is composed of several proteins. In this work, titin is considered to play the dominant role. Experimental tension-sarcomere length data [128] for a single rabbit skeletal muscle fiber was fitted using a parabolic function (Figure A.3) and scaled to make it compatible to the stress-strain characteristics of the contractile part.

$$\sigma_{22_{contr}}(\epsilon_{22}) = t_1 \epsilon_{22}^2 + t_2 \epsilon_{22} + t_3 \; for \; \epsilon_{22} > 0 \; and \tag{A.8}$$

$$\sigma_{22_{contr}}(\epsilon_{22}) = 0 \; for \; \epsilon_{22} < 0 \tag{A.9}$$

where $t_1$, $t_2$, and $t_3$ are constants.

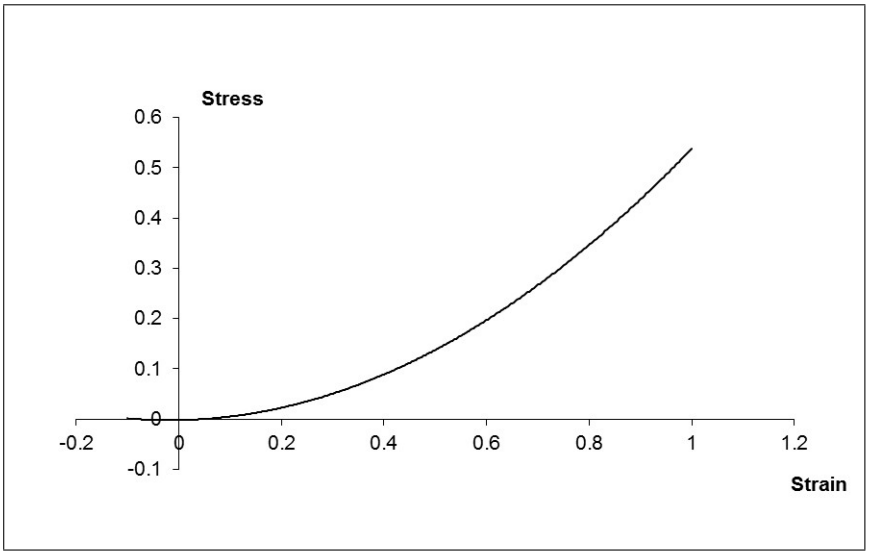



**Figure A.3** Mechanical properties representing the titin filaments which is dominating the passive resistance in the myofiber element valid only in the local fiber direction.

### A.0.3 Aponeurosis Element

In order to represent the aponeuroses, a standard 3D, 8-node element HYPER58, from the element library of ANSYS 9.0 is used. This element has a hyperelastic mechanical formulation for which the strain energy density function is defined using the two parameter Mooney-Rivlin material law:

$$W = a_{10}(\overline{I}_1 - 3) + a_{01}(\overline{I}_2 - 3) + \frac{K}{2}(\overline{I}_3 - 1)^2 \tag{A.10}$$

where, $\overline{I}_i$ are reduced invariants of right-Cauchy strain tensor for $i = 1, ..., 3$, $a_{10}$ and $a_{01}$ are Mooney-Rivlin material constants, $K = 2(a_{10} + a_{01})/(1 - 2\nu)$ is the bulk modulus and $\nu$ is the Poisson's ratio. The parameters used (Table 5.1) ensure sufficient stiffness for the aponeuroses for a representative role in force transmission and providing muscular integrity as in real muscle.

It is assumed that, at the initial muscle length in the passive state, the sarcom-

eres arranged in series within muscle fibers have identical lengths. Fiber direction strain within the fiber mesh allows assessment of the non-uniformity of lengths of sarcomeres: positive strain reflects lengthening and negative strain reflects shortening. Note that zero strain represents the undeformed state of sarcomeres (i.e., sarcomere length: 2.5 ) in the passive condition at initial muscle length. Model results obtained for muscle length equaling 25.2 mm (referred to as low muscle length) as well as muscle optimum length were studied in particular.

### A.0.4 Model of Isolated Intact EDL Muscle

EDL muscle of the rat was modeled. This muscle has a relatively simple geometry: it is a unipennate muscle with rather small pennation angles and minimal variation of the fiber direction within the muscle belly. The geometry of the model is defined as the contour of a longitudinal slice at the middle of the isolated rat EDL muscle belly. Three muscle elements in series and sixteen in parallel fill this slice. All aponeurosis elements have identical mechanical properties but using a variable thickness in the fiber-cross fiber plane, the increasing cross-sectional area of the aponeurosis toward the tendon is accounted for [123]. This model (referred to as non-paralyzed muscle) was studied after the entire muscle elements were activated maximally (for a description of the activation procedure see [27]). Three fundamental muscle data are collected from the models: Length-force relationship, strain distribution and stress distribution. Length-force data usually can not be obtained for the entire active range of motion, therefore is extrapolated at low lengths. For this purpose curve fitting toolbox of Matlab was used. Note that the model generated and described by Yucesoy et al. [27] has been validated with experimental data and a finer mesh is created in accordance with this model. The reliability of the new model is confirmed by comparison with previous mesh and presented in the results section.

# REFERENCES


1. Cosgrove, A. P., and H. K. Graham, "Botulinum toxin a prevents the development of contractures in the hereditary spastic mouse," *Dev Med Child Neurol*, Vol. 36, no. 5, pp. 379–85, 1994.

2. Jankovic, J., A. Esquenazi, D. Fehlings, F. Freitag, A. M. Lang, and M. Naumann, "Evidence-based review of patient-reported outcomes with botulinum toxin type a," *Clin Neuropharmacol*, Vol. 27, no. 5, pp. 234–44, 2004.

3. Criswell, S. R., B. E. Crowner, and B. A. Racette, "The use of botulinum toxin therapy for lower-extremity spasticity in children with cerebral palsy," *Neurosurg Focus*, Vol. 21, no. 2, p. e1, 2006.

4. Brin, M. F., "Botulinum toxin: chemistry, pharmacology, toxicity, and immunology," *Muscle Nerve Suppl*, Vol. 6, pp. S146–68, 1997.

5. Shaari, C. M., E. George, B. L. Wu, H. F. Biller, and I. Sanders, "Quantifying the spread of botulinum toxin through muscle fascia," *Laryngoscope*, Vol. 101, no. 9, pp. 960–4, 1991.

6. Borodic, G. E., R. Ferrante, L. B. Pearce, and K. Smith, "Histologic assessment of dose-related diffusion and muscle fiber response after therapeutic botulinum a toxin injections," *Mov Disord*, Vol. 9, no. 1, pp. 31–9, 1994.

7. Metezeau, P., and M. Desban, "Botulinum toxin type a: kinetics of calcium dependent paralysis of the neuromuscular junction and antagonism by drugs and animal toxins," *Toxicon*, Vol. 20, no. 3, pp. 649–54, 1982.

8. Kim, Y. I., T. Lomo, M. T. Lupa, and S. T hesleff, "Miniature end-plate potentials in rat skeletal muscle poisoned with botulinum toxin," *J Physiol*, Vol. 356, pp. 587–99, 1984.

9. Shaari, C. M., and I. Sanders, "Quantifying how location and dose of botulinum toxin injections affect muscle paralysis," *Muscle Nerve*, Vol. 16, no. 9, pp. 964–9, 1993.

10. Yaraskavitch, M., T. Leonard, and W. Herzog, "Botox produces functional weakness in non-injected muscles adjacent to the target muscle," *J Biomech*, Vol. 41, no. 4, pp. 897–902, 2008.

11. Yucesoy, C. A., O. E. Arikan, and F. Ates, "Btx-a administration to the target muscle affects forces of all muscles within an intact compartment and epimuscular myofascial force transmission," *Journal of Biomechanical Engineering*, Vol. 134, pp. 111002–1–9, 2012.

12. Longino, D., C. Frank, and W. Herzog, "Acute botulinum toxin-induced muscle weakness in the anterior cruciate ligament-deficient rabbit," *Journal of Orthopaedic Research*, Vol. 23, no. 6, pp. 1404–10, 2005.

13. Rehan Youssef, A., D. Longino, R. Seerattan, T. Leonard, and W. Herzog, "Muscle weakness causes joint degeneration in rabbits," *Osteoarthritis Cartilage*, Vol. 17, no. 9, pp. 1228–35, 2009.

14. Fortuna, R., M. A. Vaz, A. R. Youssef, D. Longino, and W. Herzog, "Changes in contractile properties of muscles receiving repeat injections of botulinum toxin (botox)," *J Biomech*, Vol. 44, no. 1, pp. 39–44, 2011.

15. Longino, D., T. A. Butterfield, and W. Herzog, "Frequency and length-dependent effects of botulinum toxin-induced muscle weakness," *J Biomech*, Vol. 38, no. 3, pp. 609–13, 2005.

16. Dimitrova, D. M., M. S. Shall, and S. J. Goldberg, "Short-term effects of botulinum toxin on the lateral rectus muscle of the cat," *Exp Brain Res*, Vol. 147, no. 4, pp. 449–55, 2002.

17. Berthier, C., and S. Blaineau, "Supramolecular organization of the subsarcolemmal cytoskeleton of adult skeletal muscle fibers. a review," *Biology of the Cell*, Vol. 89, no. 7, pp. 413–34, 1997.

18. Hawkins, D., and M. Bey, "Muscle and tendon force-length properties and their interactions in vivo," *J Biomech*, Vol. 30, no. 1, pp. 63–70, 1997.

19. Lieber, R. L., B. O. Ljung, and J. Friden, "Intraoperative sarcomere length measurements reveal differential design of human wrist extensor muscles," *J Exp Biol*, Vol. 200, no. Pt 1, pp. 19–25, 1997.

20. Ramsey, R. W., and S. F. Street, "The isometric length-tension diagram of isolated skeletal muscle fibers of the frog," *Journal of Cellular and Comparative Physiology*, Vol. 15, no. 1, pp. 11–34, 1940.

21. Street, S. F., "Lateral transmission of tension in frog myofibers: a myofibrillar network and transverse cytoskeletal connections are possible transmitters," *Journal of Cellular Physiology*, Vol. 114, no. 3, pp. 346–64, 1983.

22. Street, S. F., and R. W. Ramsey, "Sarcolemma: transmitter of active tension in frog skeletal muscle," *Science*, Vol. 149, no. 3690, pp. 1379–80, 1965.

23. Huijing, P. A., G. C. Baan, and G. T. Rebel, "Non-myotendinous force transmission in rat extensor digitorum longus muscle," *J Exp Biol*, Vol. 201, no. Pt 5, pp. 683–91, 1998.

24. Huijing, P. A., "Muscle, the motor of movement: properties in function, experiment and modelling," *J Electromyogr Kinesiol*, Vol. 8, no. 2, pp. 61–77, 1998.

25. Huijing, P. A., "Muscle as a collagen fiber reinforced composite: a review of force transmission in muscle and whole limb," *J Biomech*, Vol. 32, no. 4, pp. 329–45, 1999.

26. Trotter, J. A., and P. P. Purslow, "Functional morphology of the endomysium in series fibered muscles," *J Morphol*, Vol. 212, no. 2, pp. 109–22, 1992.

27. Yucesoy, C. A., B. H. Koopman, P. A. Huijing, and H. J. Grootenboer, "Three-dimensional finite element modeling of skeletal muscle using a two-domain approach: linked fiber-matrix mesh model," *Journal of Biomechanics*, Vol. 35, no. 9, pp. 1253–62, 2002.

28. Willems, M. E., and P. A. Huijing, "Heterogeneity of mean sarcomere length in different fibres: effects on length range of active force production in rat muscle," *Eur J Appl Physiol Occup Physiol*, Vol. 68, no. 6, pp. 489–96, 1994.

29. Yucesoy, C. A., B. H. Koopman, G. C. Baan, H. J. Grootenboer, and P. A. Huijing, "Effects of inter- and extramuscular myofascial force transmission on adjacent synergistic muscles: assessment by experiments and finite-element modeling," *J Biomech*, Vol. 36, no. 12, pp. 1797–811, 2003.

30. Yucesoy, C. A., and P. A. Huijing, "Substantial effects of epimuscular myofascial force transmission on muscular mechanics have major implications on spastic muscle and remedial surgery," *Journal of Electromyography and Kinesiology*, Vol. 17, no. 6, pp. 664–79, 2007.

31. Huijing, P. A., and G. C. Baan, "Extramuscular myofascial force transmission within the rat anterior tibial compartment: proximo-distal differences in muscle force," *Acta Physiol Scand*, Vol. 173, no. 3, pp. 297–311, 2001.

32. Maas, H., G. C. Baan, and P. A. Huijing, "Intermuscular interaction via myofascial force transmission: effects of tibialis anterior and extensor hallucis longus length on force transmission from rat extensor digitorum longus muscle," *J Biomech*, Vol. 34, no. 7, pp. 927–40, 2001.

33. Yucesoy, C. A., G. C. Baan, B. H. Koopman, H. J. Grootenboer, and P. A. Huijing, "Pre-strained epimuscular connections cause muscular myofascial force transmission to affect properties of synergistic ehl and edl muscles of the rat," *J Biomech Eng*, Vol. 127, no. 5, pp. 819–28, 2005.

34. Yucesoy, C. A., B. H. Koopman, G. C. Baan, H. J. Grootenboer, and P. A. Huijing, "Extramuscular myofascial force transmission: experiments and finite element modeling," *Arch Physiol Biochem*, Vol. 111, no. 4, pp. 377–88, 2003.

35. Huijing, P. A., A. Yaman, C. Ozturk, and C. A. Yucesoy, "Effects of knee joint angle on global and local strains within human triceps surae muscle: Mri analysis indicating in vivo myofascial force transmission between synergistic muscles," *Surg Radiol Anat*, Vol. 33, no. 10, pp. 869–79, 2011.

36. Maas, H., G. C. Baan, P. A. Huijing, C. A. Yucesoy, B. H. Koopman, and H. J. Grootenboer, "The relative position of edl muscle affects the length of sarcomeres within muscle fibers: experimental results and finite-element modeling," *J Biomech Eng*, Vol. 125, no. 5, pp. 745–53, 2003.

37. Meijer, H. J., J. M. Rijkelijkhuizen, and P. A. Huijing, "Myofascial force transmission between antagonistic rat lower limb muscles: effects of single muscle or muscle group lengthening," *J Electromyogr Kinesiol*, Vol. 17, no. 6, pp. 698–707, 2007.

38. Yucesoy, C. A., B. H. Koopman, H. J. Grootenboer, and P. A. Huijing, "Finite element modeling of aponeurotomy: altered intramuscular myofascial force transmission yields complex sarcomere length distributions determining acute effects," *Biomech Model Mechanobiol*, Vol. 6, no. 4, pp. 227–43, 2007.

39. Yucesoy, C. A., H. Maas, B. H. Koopman, H. J. Grootenboer, and P. A. Huijing, "Mechanisms causing effects of muscle position on proximo-distal muscle force differences in extra-muscular myofascial force transmission," *Med Eng Phys*, Vol. 28, no. 3, pp. 214–26, 2006.

40. Gracies, J. M., "Pathophysiology of spastic paresis. ii: Emergence of muscle overactivity," *Muscle Nerve*, Vol. 31, no. 5, pp. 552–71, 2005.

41. Botte, M. J., V. L. Nickel, and W. H. Akeson, "Spasticity and contracture. physiologic aspects of formation," *Clin Orthop Relat Res*, no. 233, pp. 7–18, 1988.

42. Feldman, R., R. Young, and W. Koella, "Spasticity: Disordered motor control.," *Symposia Specialists, Incorporated.*, 1980.

43. Sanger, T. D., M. R. Delgado, D. Gaebler-Spira, M. Hallett, and J. W. Mink, "Classification and definition of disorders causing hypertonia in childhood," *Pediatrics*, Vol. 111, no. 1, pp. e89–97, 2003.

44. Filippi, G. M., P. Errico, R. Santarelli, B. Bagolini, and E. Manni, "Botulinum a toxin effects on rat jaw muscle spindles," *Acta Oto-laryngologica*, Vol. 113, no. 3, pp. 400–4, 1993.

45. Giladi, N., "The mechanism of action of botulinum toxin type a in focal dystonia is most probably through its dual effect on efferent (motor) and afferent pathways at the injected site," *Journal of the Neurological Sciences*, Vol. 152, no. 2, pp. 132–5, 1997.

46. Rosales, R. L., K. Arimura, S. Takenaga, and M. Osame, "Extrafusal and intrafusal muscle effects in experimental botulinum toxin-a injection," *Muscle Nerve*, Vol. 19, no. 4, pp. 488–96, 1996.

47. Anwar, K., and M. P. Barnes, "Botulinum toxin injections for spasticity," *Operative Techniques in Neurosurgery*, Vol. 7, no. 3, pp. 128 – 135, 2004.

48. Cardoso, E. S., B. M. Rodrigues, M. Barroso, C. J. Menezes, R. S. Lucena, D. B. Nora, and A. Melo, "Botulinum toxin type a for the treatment of the spastic equinus foot in cerebral palsy," *Pediatr Neurol*, Vol. 34, no. 2, pp. 106–9, 2006.

49. Lukban, M. B., R. L. Rosales, and D. Dressler, "Effectiveness of botulinum toxin a for upper and lower limb spasticity in children with cerebral palsy: a summary of evidence," *J Neural Transm*, Vol. 116, no. 3, pp. 319–31, 2009.

50. Molenaers, G., V. Schorkhuber, K. Fagard, A. Van Campenhout, J. De Cat, P. Pauwels, E. Ortibus, P. De Cock, and K. Desloovere, "Long-term use of botulinum toxin type a in children with cerebral palsy: treatment consistency," *Eur J Paediatr Neurol*, Vol. 13, no. 5, pp. 421–9, 2009.

51. Burgen, A. S., F. Dickens, and L. J. Zatman, "The action of botulinum toxin on the neuro-muscular junction," *J Physiol*, Vol. 109, no. 1-2, pp. 10–24, 1949.

52. Esquenazi, A., and N. Mayer, "Botulinum toxin for the management of muscle overactivity and spasticity after stroke," *Curr Atheroscler Rep*, Vol. 3, no. 4, pp. 295–8, 2001.

53. Sheean, G. L., "Botulinum treatment of spasticity: why is it so difficult to show a functional benefit?," *Current Opinion in Neurology*, Vol. 14, no. 6, pp. 771–6, 2001.

54. Cichon, J. V., J., T. V. McCaffrey, W. J. Litchy, and J. L. Knops, "The effect of botulinum toxin type a injection on compound muscle action potential in an in vivo rat model," *Laryngoscope*, Vol. 105, no. 2, pp. 144–8, 1995.

55. Ates, F., and C. A. Yucesoy, "Effects of botulinum toxin type a on non-injected biarticular muscle include a narrower length range of force exertion and increased passive force," *Muscle and Nerve*, Vol. 49, no. 6, pp. 866–878, 2014.

56. Yucesoy, C. A., "Epimuscular myofascial force transmission implies novel principles for muscular mechanics," *Exercise and Sport Sciences Reviews*, Vol. 38, no. 3, pp. 128–34, 2010.

57. Nishimura, T., A. Hattori, and K. Takahashi, "Arrangement and identification of proteoglycans in basement membrane and intramuscular connective tissue of bovine semitendinosus muscle," *Acta Anatomica (Basel)*, Vol. 155, no. 4, pp. 257–65, 1996.

58. Passerieux, E., R. Rossignol, T. Letellier, and J. P. Delage, "Physical continuity of the perimysium from myofibers to tendons: involvement in lateral force transmission in skeletal muscle," *J Struct Biol*, Vol. 159, no. 1, pp. 19–28, 2007.

59. Maas, H., G. C. Baan, and P. A. Huijing, "Muscle force is determined also by muscle relative position: isolated effects," *J Biomech*, Vol. 37, no. 1, pp. 99–110, 2004.

60. Huijing, P. A., H. Maas, and G. C. Baan, "Compartmental fasciotomy and isolating a muscle from neighboring muscles interfere with myofascial force transmission within the rat anterior crural compartment," *J Morphol*, Vol. 256, no. 3, pp. 306–21, 2003.

61. Huijing, P. A., "Epimuscular myofascial force transmission: A historical review and implications for new research. international society of biomechanics muybridge award lecture, taipei, 2007," *Journal of Biomechanics*, Vol. 42, no. 1, pp. 9–21, 2009.

62. Bojsen-Moller, J., S. Schwartz, K. K. Kalliokoski, T. Finni, and S. P. Magnusson, "Intermuscular force transmission between human plantarflexor muscles in vivo," *J Appl Physiol*, Vol. 109, no. 6, pp. 1608–18, 2010.

63. Carvalhais, V. O., M. Ocarino Jde, V. L. Araujo, T. R. Souza, P. L. Silva, and S. T. Fonseca, "Myofascial force transmission between the latissimus dorsi and gluteus maximus muscles: An in vivo experiment," *J Biomech*, Vol. 46, no. 5, pp. 1003–7, 2013.

64. Oda, T., H. Kanehisa, K. Chino, T. Kurihara, T. Nagayoshi, T. Fukunaga, and Y. Kawakami, "In vivo behavior of muscle fascicles and tendinous tissues of human gastrocnemius and soleus muscles during twitch contraction," *J Electromyogr Kinesiol*, Vol. 17, no. 5, pp. 587–95, 2007.

65. Yaman, A., C. Ozturk, P. A. Huijing, and C. A. Yucesoy, "Magnetic resonance imaging assessment of mechanical interactions between human lower leg muscles in vivo," *J Biomech Eng*, Vol. 135, no. 9, pp. 91003–9, 2013.

66. Huijing, P. A., "Epimuscular myofascial force transmission between antagonistic and synergistic muscles can explain movement limitation in spastic paresis," *J Electromyogr Kinesiol*, Vol. 17, no. 6, pp. 708–24, 2007.

67. Ates, F., Y. Temelli, and C. A. Yucesoy, "Human spastic gracilis muscle isometric forces measured intraoperatively as a function of knee angle show no abnormal muscular mechanics," *Clin Biomech (Bristol, Avon)*, Vol. 28, no. 1, pp. 48–54, 2013.

68. Yucesoy, C. A., and P. A. Huijing, "Assessment by finite element modeling indicates that surgical intramuscular aponeurotomy performed closer to the tendon enhances intended acute effects in extramuscularly connected muscle," *J Biomech Eng*, Vol. 131, no. 2, p. 021012, 2009.

69. Yucesoy, C. A., B. H. Koopman, H. J. Grootenboer, and P. A. Huijing, "Extramuscular myofascial force transmission alters substantially the acute effects of surgical aponeurotomy: assessment by finite element modeling," *Biomechanics and Modeling in Mechanobiology*, Vol. 7, no. 3, pp. 175–89, 2008.

70. Ates, F., R. N. Ozdeslik, P. Huijing, and Y. C. A., "Muscle lengthening surgery causes differential acute mechanical effects in both targeted and non-targeted synergistic muscles," *Journal of Electromyography and Kinesiology*, Vol. in press, 2013.

71. Cleland, J., "On the actions of muscles passing over more than one joint," *J Anat Physiol*, Vol. 1, no. 1, pp. 85–93, 1867.

72. Borodic, G. E., M. Joseph, L. Fay, D. Cozzolino, and R. J. Ferrante, "Botulinum a toxin for the treatment of spasmodic torticollis: dysphagia and regional toxin spread," *Head Neck*, Vol. 12, no. 5, pp. 392–9, 1990.

73. Kuehn, B. M., "Studies, reports say botulinum toxins may have effects beyond injection site," *JAMA*, Vol. 299, no. 19, pp. 2261–3, 2008.

74. Neter, J., M. H. Kutner, C. J. Nachtsheim, and W. Wasserman, *Applied linear statistical models*, Irwin, Homewood, IL.: McGraw-Hill/Irwin; 4 edition, 1996.

75. Turkoglu, A. N., P. A. Huijing, and C. A. Yucesoy, "Mechanical principles of effects of botulinum toxin on muscle length-force characteristics: An assessment by finite element modeling," *Journal of Biomechanics*, Vol. 47, no. 7, pp. 1565–71, 2014.

76. Yucesoy, C. A., A. N. Turkoglu, S. Umur, and F. Ates, "Intact muscle compartment exposed to botulinum toxin type a shows compromised intermuscular mechanical interaction," *Muscle Nerve*, Vol. 51, no. 1, pp. 106–16, 2015.

77. Boyd, R. N., and H. K. Graham, "Objective measurement of clinical findings in the use of botulinum toxin type a for the management of children with cerebral palsy," *European Journal of Neurology*, Vol. 6, pp. s23–s35, 1999.

78. Kay, R. M., S. A. Rethlefsen, A. Fern-Buneo, T. A. Wren, and D. L. Skaggs, "Botulinum toxin as an adjunct to serial casting treatment in children with cerebral palsy," *J Bone Joint Surg Am*, Vol. 86-A, no. 11, pp. 2377–84, 2004.

79. Huyghe, J. M., D. H. van Campen, T. Arts, and R. M. Heethaar, "A two-phase finite element model of the diastolic left ventricle," *Journal of Biomechanics*, Vol. 24, pp. 527–538, 1991.

80. Yucesoy, C. A., and P. A. Huijing, "Specifically tailored use of the finite element method to study muscular mechanics within the context of fascial integrity: The linked fiber-matrix mesh model," *International Journal for Multiscale Computational Engineering*, Vol. 10, no. 155-170, 2012.

81. Jaspers, R. T., R. Brunner, J. J. Pel, and P. A. Huijing, "Acute effects of intramuscular aponeurotomy on rat gastrocnemius medialis: force transmission, muscle force and sarcomere length," *Journal of Biomechanics*, Vol. 32, no. 1, pp. 71–9, 1999.

82. Satila, H., T. Pietikainen, T. Iisalo, P. Lehtonen-Raty, M. Salo, R. Haataja, M. Koivikko, and I. Autti-Ramo, "Botulinum toxin type a injections into the calf muscles for treatment of spastic equinus in cerebral palsy: a randomized trial comparing single and multiple injection sites," *Am J Phys Med Rehabil*, Vol. 87, no. 5, pp. 386–94, 2008.

83. Brown, J. K., J. Rodda, E. G. Walsh, and G. W. Wright, "Neurophysiology of lower-limb function in hemiplegic children," *Dev Med Child Neurol*, Vol. 33, no. 12, pp. 1037–47, 1991.

84. Mirbagheri, M. M., H. Barbeau, M. Ladouceur, and R. E. Kearney, "Intrinsic and reflex stiffness in normal and spastic, spinal cord injured subjects," *Exp Brain Res*, Vol. 141, no. 4, pp. 446–59, 2001.

85. O'Dwyer, N. J., and L. Ada, "Reflex hyperexcitability and muscle contracture in relation to spastic hypertonia," *Curr Opin Neurol*, Vol. 9, no. 6, pp. 451–5, 1996.

86. Hesse, S., J. Krajnik, D. Luecke, M. T. Jahnke, M. Gregoric, and K. H. Mauritz, "Ankle muscle activity before and after botulinum toxin therapy for lower limb extensor spasticity in chronic hemiparetic patients," *Stroke*, Vol. 27, no. 3, pp. 455–60, 1996.

87. Strumpf, R. K., J. D. Humphrey, and F. C. Yin, "Biaxial mechanical properties of passive and tetanized canine diaphragm," *Am J Physiol*, Vol. 265, no. 2 Pt 2, pp. H469–75, 1993.

88. Billante, C. R., D. L. Zealear, M. Billante, J. H. Reyes, G. Sant'Anna, R. Rodriguez, and J. Stone, R. E., "Comparison of neuromuscular blockade and recovery with botulinum toxins a and f," *Muscle Nerve*, Vol. 26, no. 3, pp. 395–403, 2002.

89. Cans, C., "Surveillance of cerebral palsy in europe: a collaboration of cerebral palsy surveys and registers," *Developmental Medicine  Child Neurology*, Vol. 42, no. 12, pp. 816–824, 2000.

90. Sheean, G., and J. R. McGuire, "Spastic hypertonia and movement disorders: pathophysiology, clinical presentation, and quantification," *PM R*, Vol. 1, no. 9, pp. 827–33, 2009.

91. Harlaar, J., J. G. Becher, C. J. Snijders, and G. J. Lankhorst, "Passive stiffness characteristics of ankle plantar flexors in hemiplegia," *Clinical biomechanics (Bristol, Avon)*, Vol. 15, no. 4, pp. 261–70, 2000.

92. Koman, L. A., r. Mooney, J. F., B. Smith, A. Goodman, and T. Mulvaney, "Management of cerebral palsy with botulinum-a toxin: preliminary investigation," *J Pediatr Orthop*, Vol. 13, no. 4, pp. 489–95, 1993.

93. Esquenazi, A., I. Novak, G. Sheean, B. J. Singer, and A. B. Ward, "International consensus statement for the use of botulinum toxin treatment in adults and children with neurological impairments–introduction," *Eur J Neurol*, Vol. 17 Suppl 2, pp. 1–8, 2010.

94. Olver, J., A. Esquenazi, V. S. Fung, B. J. Singer, A. B. Ward, and I. Cerebral Palsy, "Botulinum toxin assessment, intervention and aftercare for lower limb disorders of movement and muscle tone in adults: international consensus statement," *Eur J Neurol*, Vol. 17 Suppl 2, pp. 57–73, 2010.

95. Frasson, E., E. Dall'ora, M. Bordignon, F. Brigo, P. Tocco, D. Primon, G. Didone, S. Vicentini, A. Fiaschi, and L. Bertolasi, "Spread of botulinum neurotoxin type a at standard doses is inherent to the successful treatment of spastic equinus foot in cerebral palsy: short-term neurophysiological and clinical study," *J Child Neurol*, Vol. 27, no. 5, pp. 587–93, 2012.

96. Koman, L. A., B. P. Smith, and J. S. Shilt, "Cerebral palsy," *Lancet*, Vol. 363, no. 9421, pp. 1619–31, 2004.

97. Graham, H. K., K. R. Aoki, I. Autti-Ramo, R. N. Boyd, M. R. Delgado, D. J. Gaebler-Spira, M. E. Gormley, B. M. Guyer, F. Heinen, A. F. Holton, D. Matthews, G. Molenaers, F. Motta, P. J. Garcia Ruiz, and J. Wissel, "Recommendations for the use of botulinum

toxin type a in the management of cerebral palsy," *Gait Posture*, Vol. 11, no. 1, pp. 67–79, 2000.

98. Hamdy, R. C., K. Montpetit, J. Ruck-Gibis, K. Thorstad, E. Raney, M. Aiona, R. Platt, A. Finley, W. Mackenzie, J. McCarthy, and U. Narayanan, "Safety and efficacy of botox injection in alleviating post-operative pain and improving quality of life in lower extremity limb lengthening and deformity correction," *Trials*, Vol. 8, p. 27, 2007.

99. Hyman, N., M. Barnes, B. Bhakta, A. Cozens, M. Bakheit, B. Kreczy-Kleedorfer, W. Poewe, J. Wissel, P. Bain, S. Glickman, A. Sayer, A. Richardson, and C. Dott, "Botulinum toxin (dysport) treatment of hip adductor spasticity in multiple sclerosis: a prospective, randomised, double blind, placebo controlled, dose ranging study," *J Neurol Neurosurg Psychiatry*, Vol. 68, no. 6, pp. 707–12, 2000.

100. Gracies, J. M., "Pathophysiology of spastic paresis. i: Paresis and soft tissue changes," *Muscle Nerve*, Vol. 31, no. 5, pp. 535–51, 2005.

101. Bakheit, A. M., A. F. Thilmann, A. B. Ward, W. Poewe, J. Wissel, J. Muller, R. Benecke, C. Collin, F. Muller, C. D. Ward, and C. Neumann, "A randomized, double-blind, placebo-controlled, dose-ranging study to compare the efficacy and safety of three doses of botulinum toxin type a (dysport) with placebo in upper limb spasticity after stroke," *Stroke*, Vol. 31, no. 10, pp. 2402–6, 2000.

102. Van Der Walt, A., S. Sung, T. Spelman, M. Marriott, S. Kolbe, P. Mitchell, A. Evans, and H. Butzkueven, "A double-blind, randomized, controlled study of botulinum toxin type a in ms-related tremor," *Neurology*, Vol. 79, no. 1, pp. 92–9, 2012.

103. Kreulen, M., M. J. Smeulders, J. J. Hage, and P. A. Huijing, "Biomechanical effects of dissecting flexor carpi ulnaris," *J Bone Joint Surg Br*, Vol. 85, no. 6, pp. 856–9, 2003.

104. Ates, F., Y. Temelli, and C. A. Yucesoy, "Intraoperative experiments show relevance of inter-antagonistic mechanical interaction for spastic muscle's contribution to joint movement disorder," *Clin Biomech (Bristol, Avon)*, Vol. 29, no. 8, pp. 943–9, 2014.

105. Gruner, J. A., J. Altman, and N. Spivack, "Effects of arrested cerebellar development on locomotion in the rat. cinematographic and electromyographic analysis," *Exp Brain Res*, Vol. 40, no. 4, pp. 361–73, 1980.

106. Lichtwark, G. A., K. Bougoulias, and A. M. Wilson, "Muscle fascicle and series elastic element length changes along the length of the human gastrocnemius during walking and running," *J Biomech*, Vol. 40, no. 1, pp. 157–64, 2007.

107. Elder, G. C., J. Kirk, G. Stewart, K. Cook, D. Weir, A. Marshall, and L. Leahey, "Contributing factors to muscle weakness in children with cerebral palsy," *Dev Med Child Neurol*, Vol. 45, no. 8, pp. 542–50, 2003.

108. Mahant, N., P. D. Clouston, and I. T. Lorentz, "The current use of botulinum toxin," *J Clin Neurosci*, Vol. 7, no. 5, pp. 389–94, 2000.

109. Sinkjaer, T., and I. Magnussen, "Passive, intrinsic and reflex-mediated stiffness in the ankle extensors of hemiparetic patients," *Brain*, Vol. 117 ( Pt 2), pp. 355–63, 1994.

110. Tardieu, C., E. Huet de la Tour, M. D. Bret, and G. Tardieu, "Muscle hypoextensibility in children with cerebral palsy: I. clinical and experimental observations," *Archives of Physical Medicine and Rehabilitation*, Vol. 63, no. 3, pp. 97–102, 1982.

111. Booth, C. M., M. J. Cortina-Borja, and T. N. Theologis, "Collagen accumulation in muscles of children with cerebral palsy and correlation with severity of spasticity," *Dev Med Child Neurol*, Vol. 43, no. 5, pp. 314–20, 2001.

112. Mohagheghi, A. A., T. Khan, T. H. Meadows, K. Giannikas, V. Baltzopoulos, and C. N. Maganaris, "In vivo gastrocnemius muscle fascicle length in children with and without diplegic cerebral palsy," *Dev Med Child Neurol*, Vol. 50, no. 1, pp. 44–50, 2008.

113. Malaiya, R., A. E. McNee, N. R. Fry, L. C. Eve, M. Gough, and A. P. Shortland, "The morphology of the medial gastrocnemius in typically developing children and children with spastic hemiplegic cerebral palsy," *J Electromyogr Kinesiol*, Vol. 17, no. 6, pp. 657–63, 2007.

114. Smith, L. R., K. S. Lee, S. R. Ward, H. G. Chambers, and R. L. Lieber, "Hamstring contractures in children with spastic cerebral palsy result from a stiffer extracellular matrix and increased in vivo sarcomere length," *J Physiol*, Vol. 589, no. Pt 10, pp. 2625–39, 2011.

115. Borodic, G. E., L. B. Pearce, K. Smith, and M. Joseph, "Botulinum a toxin for spasmodic torticollis: multiple vs single injection points per muscle," *Head and Neck*, Vol. 14, no. 1, pp. 33–7, 1992.

116. Kalandakanond, S., and J. A. Coffield, "Cleavage of snap-25 by botulinum toxin type a requires receptor-mediated endocytosis, ph-dependent translocation, and zinc," *J Pharmacol Exp Ther*, Vol. 296, no. 3, pp. 980–6, 2001.

117. Brooks, V. B., "The action of botulinum toxin on motor-nerve filaments," *J Physiol*, Vol. 123, no. 3, pp. 501–15, 1954.

118. Lalli, G., J. Herreros, S. L. Osborne, C. Montecucco, O. Rossetto, and G. Schiavo, "Functional characterisation of tetanus and botulinum neurotoxins binding domains," *J Cell Sci*, Vol. 112 ( Pt 16), pp. 2715–24, 1999.

119. Eng, C. M., L. H. Smallwood, M. P. Rainiero, M. Lahey, S. R. Ward, and R. L. Lieber, "Scaling of muscle architecture and fiber types in the rat hindlimb," *J Exp Biol*, Vol. 211, no. Pt 14, pp. 2336–45, 2008.

120. Ward, S. R., C. M. Eng, L. H. Smallwood, and R. L. Lieber, "Are current measurements of lower extremity muscle architecture accurate?," *Clin Orthop Relat Res*, Vol. 467, no. 4, pp. 1074–82, 2009.

121. Heslinga, J. W., and P. A. Huijing, "Muscle length-force characteristics in relation to muscle architecture: a bilateral study of gastrocnemius medialis muscles of unilaterally immobilized rats," *Eur J Appl Physiol Occup Physiol*, Vol. 66, no. 4, pp. 289–98, 1993.

122. Jarvinen, T. A., L. Jozsa, P. Kannus, T. L. Jarvinen, and M. Jarvinen, "Organization and distribution of intramuscular connective tissue in normal and immobilized skeletal muscles. an immunohistochemical, polarization and scanning electron microscopic study," *J Muscle Res Cell Motil*, Vol. 23, no. 3, pp. 245–54, 2002.

123. Zuurbier, C. J., A. J. Everard, P. V. der Wees, and P. A. Huijing, "Length-force characteristics of the aponeurosis in the passive and active muscle condition and in the isolated condition," *Journal of Biomechanics*, Vol. 27, pp. 445–453, 1994.

124. Maganaris, C. N., and J. P. Paul, "In vivo human tendon mechanical properties," *J Physiol*, Vol. 521 Pt 1, pp. 307–13, 1999.

125. Edstrom, L., and E. Kugelberg, "Histochemical composition, distribution of fibres and fatiguability of single motor units. anterior tibial muscle of the rat," *J Neurol Neurosurg Psychiatry*, Vol. 31, no. 5, pp. 424–33, 1968.

126. Yucesoy, C. A., *Intra-, inter- and extra-muscular myofascial force transmission: A combined finite element modeling and experimental approach.* PhD thesis, University of Twente, Utrecht, The Netherlands, 2003.

127. Zuurbier, C. J., J. W. Heslinga, M. B. L. de Groot, and W. J. V. der Laarse, "Mean sarcomere length-force relationship of rat muscle fiber bundles," *Journal of Biomechanics*, Vol. 28, pp. 83–87, 1995.

128. Trombitas, K., J. P. Jin, and H. Granzier, "The mechanically active domain of titin in cardiac muscle," *Circulation Research*, Vol. 77, pp. 856–861, 1995.